Thermodynamic analysis and heat exchanger calculations of transcritical high-temperature heat pumps
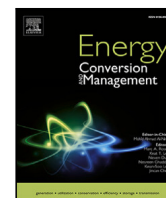
Zhao, An; Pecnik, Rene; Peeters, Jurriaan W.R.

Important note
To cite this publication, please use the final published version (if applicable).
Please check the document version above.

Research Paper

Thermodynamic analysis and heat exchanger calculations of transcritical high-temperature heat pumps

An Zhao [*], Rene Pecnik, Jurriaan W.R. Peeters

Department of Energy and Process, TU Delft, Delft 2628 CN, Netherlands

ARTICLE INFO

ABSTRACT

Heating in industrial processes is responsible for approximately 13% of greenhouse gas emissions in Europe. Switching from fossil-fuel based boilers to heat pumps can help mitigate the effect of global warming. The present work proposes novel high-temperature transcritical heat pump cycles targeted at heating air with a mass flow rate of 10 kg/s up to 200 °C for spray drying processes. Four low-GWP refrigerants, R1233zd(E), R1336mzz(Z), n-Butane, and Ammonia are considered as the candidate working fluids. The pressure ratio of the compressor is optimized to achieve a maximum coefficient of performance (COP) for the four working fluids. A shell & tube heat exchanger is considered as the gas cooler. Using a generalized version of the ϵ-NTU method, the gas cooler is sized and a second law analysis is conducted. Striking a balance between the first- and second-law performance and size of the gas cooler, the R1233zd(E) transcritical heat pump cycle with a COP of 3.6 is judged to be the most promising option.

1. Introduction

In the European Union (EU), the industrial sector consumes 26% of the total energy and emits 20% of the greenhouse gas [1]. Two-thirds of the energy consumption and greenhouse gas emissions are the result of process heating [2]. Therefore, reducing energy consumption and greenhouse gas emission in heating processes would contribute significantly to achieving the EU's goal of becoming climate-neutral by 2050 [3]. Electrification is an important strategy to decarbonize process heat [4].

Adopting electric-driven heat pumps is considered a promising solution to supply process heating in an effective and sustainable way [5]. Heat pumps provide the possibility of recovering on-site waste heat [6], making their coefficient of performance (COP) significantly higher than electric boilers. Moreover, they can be retrofitted into existing process facilities by replacing fossil fuels-based heaters. However, over 89% of the process heating demand requires temperatures well over 100 °C [7]. For example, spray drying is an important process in the food industry, which requires air at a temperature of 160 to 200 °C [8]. It is widely employed in producing dairy products, such as milk powders [9].

Unfortunately, commercialized heat pumps available on the current market are operated at much lower temperatures [10]. Consequently, much work has been devoted to developing high-temperature heat pump systems in recent years [11]. It should be noted here that there is no consensus on the meaning of "high temperature" in the research community. Some researchers use this term to refer to a sink temperature higher than 75 °C [12], others use it to refer to a sink temperature higher than 110 °C [13]. Recent high-temperature heat pump research was targeted at a maximum temperature of 150 °C [14]. In this work, "high temperature" is referred to specifically as the temperature range well above 160 °C. So far, few attempts [15] have been made to develop heat pump cycles in this temperature range.

The aforementioned temperature range is above the critical temperature of many refrigerants. The latter suggests that the working fluid would be in its supercritical state in the condenser (provided the pressure is higher than the critical pressure). When the working fluid is in a supercritical state when transferring heat and in a sub-critical state when absorbing heat, the heat pump cycle is said to be "transcritical", see Fig. 1. Numerous works were already conducted to investigate trans-critical cycles, with an emphasis on carbon dioxide (CO_2) [16]. CO_2 heat pump systems possess the advantage of a smaller required pressure ratio [17] compared to other working fluids, thus alleviating the burden of compressors and increasing their efficiency. Compared to conventional sub-critical heat pump cycles, trans-critical heat pump cycles have less temperature mismatching between the working fluid and the air heat sink [18], which helps to reduce the irreversibility generated in gas coolers. Therefore, trans-critical cycles are potentially well suited to providing heat in spray drying processes.

Special attention should be paid to the gas cooler of a trans-critical heat pump, as the heat transfer characteristics of a working fluid

---

Nomenclature

Symbols

C_{min}	Smaller heat capacity of two sides in the gas cooler [W/K]
COP	Coefficient of performance [−]
COP_{Lorenz}	Lorenz coefficient of performance [−]
$c_{p,h}$	Specific heat capacity of the hot stream (test case) [J/(kg K)]
$c_{p,c}$	Specific heat capacity of the cold stream (test case) [J/(kg K)]
c_{pr}	Specific heat capacity of the refrigerant at the bulk temperature [J/(kg K)]
c_{prw}	Specific heat capacity of the refrigerant at the wall temperature [J/(kg K)]
ΔP_{gc}	Pressure drop in the gas cooler [W]
Δs	Entropy increase for different components of the heat pump [W]
$D_{ev,tube,inner}$	Inner diameter of the tube in the evaporator [m]
$D_{gc,tube,inner}$	Inner diameter of the tube in the gas cooler [m]
η	Second law efficiency of the heat pump cycle [−]
η_{comp}	Total efficiency of the compressor [−]
$f_{gc,r}$	Filonenko friction factor [m]
G_r	Mass flux of the refrigerant in the gas cooler [kg/m^2]
$h_{comp,i}$	Specific enthalpy of the refrigerant at the inlet of the compressor [J/kg]
$h_{comp,o,isen}$	Isentropic specific enthalpy of the refrigerant at the outlet of the compressor [J/kg]
$h_{comp,o}$	Real specific enthalpy of the refrigerant at the outlet of the compressor [J/kg]
h_{lg}	Latent heat of the refrigerant [J/kg]
h_r	Specific enthalpy of the refrigerant at bulk temperature [J/kg]
h_{rw}	Specific enthalpy of the refrigerant at wall temperature [J/kg]
I	Irreversibility for different components of the heat pump [W]
L_{gc}	Total length of all passes of the gas cooler [m]
$\dot{m}_a$	Mass flow rate of the air [kg/s]
$\dot{m}_r$	Mass flow rate of the refrigerant [kg/s]
n_{row}	Number of transverse row in the gas cooler [−]
NTU	Number of transfer units [−]
$P_{gc,in,a}$	Pressure of the air at the inlet of the gas cooler [Pa]
$P_{gc,in,r}$	Pressure of the refrigerant at the inlet of the gas cooler [Pa]
Q_{ev}	Total heat transfer power of the evaporator [W]
Q_{gc}	Total heat transfer power of the gas cooler [W]
S_n	Tube pitch along the direction perpendicular to the flow [m]
S_p	Tube pitch along the direction parallel to the flow [m]
s_r	Specific entropy of the refrigerant at the bulk temperature [J/K]
s_{rw}	Specific entropy of the refrigerant at the wall temperature [J/K]
T_c	Cold fluid temperature of the heat exchanger in the test case [°C]
$T_{ev,hs}$	The temperature of the heat souce supplied to the evaporator [°C]
$T_{ev,hs}$	heat source temperature in the evaporator [°C]
$\overline{T}_{gc,air}$	Entropic average of the air temperature in the gas cooler [K]
$T_{gc,in,a}$	Temperature of the air at the inlet of the gas cooler [°C]
$T_{gc,in,r}$	Temperature of the refrigerant at the inlet of the gas cooler [°C]
$T_{gc,out,a}$	Temperature of the air at the outlet of the gas cooler [°C]
$T_{gc,out,r}$	Temperature of the refrigerant at the outlet of the gas cooler [°C]
T_h	Hot fluid temperature of the heat exchanger in the test case [°C]
T_{pc}	Pseudo-critical temperature of the refrigerant [°C]
T_r	Bulk temperature of the refrigerant [°C]
T_{rw}	Wall temperature at the refrigerant side [°C]
P_t	Total heat exchange perimeter of the heat exchanger in the test case [m]
U	Total heat transfer coefficient of the gas cooler [K/(m^2 K)]
U_t	Total heat transfer coefficient of the heat exchanger in the test case [K/(m^2 K)]
u_{inf}	Incoming free stream velocity of the air [m/s]
X_{tt}	Lockhart–Martinelli parameter [−]
z	Coordinate along the axial direction of the heat exchanger in the test case [m]
β_h	Isobaric expansion coefficient of the refrigerant [1/K]
χ	Thermodynamic quality of the refrigerant [−]
ϵ	Effectiveness of heat exchanger [−]
λ_r	Thermal conductivity of the refrigerant [W/(m K)]
μ_a	Dynamic viscosity of the air at the bulk temperature [Pa s]
μ_{aw}	Dynamic viscosity of the air at the wall temperature [Pa s]
μ_g	Dynamic viscosity of the gas phase refrigerant [Pa s]
μ_l	Dynamic viscosity of the liquid phase refrigerant [Pa s]
μ_r	Dynamic viscosity of the refrigerant at the bulk temperature [Pa s]
μ_{rw}	Dynamic viscosity of the refrigerant at the wall temperature [Pa s]
v_g	Specific volume of the gas phase refrigerant [m^3/kg]

v_l	Specific volume of the liquid phase refrigerant [m³/kg]
ϕ_{ev}	Heat flux in the evaporator [W/m²]
ϕ_{gc}	Heat flux in the gas cooler [W/m²]
ρ_a	Density of the air [kg/m³]
ρ_g	Density of the gas phase refrigerant [kg/m³]
ρ_l	Density of the liquid phase refrigerant [kg/m³]
ρ_{pc}	Density of the supercritical refrigerant at the pseudocritical point [kg/m³]
ρ_r	Density of the refrigerant at the bulk temperature [kg/m³]
ρ_{rw}	Density of the refrigerant at the wall temperature [kg/m³]

at supercritical pressure differs considerably from sub-critical heat transfer characteristics. The former is attributed to the smooth- yet drastic material property variation of the supercritical fluids across the Widom line [19]. When crossing the Widom line as a result of heating, the supercritical fluid transitions from a liquid-like state to a gas-like state, which is known as the pseudo-boiling phenomenon [20], or vice versa for pseudo-condensation [21]. The specific heat capacity of a supercritical fluid shows a maximum very close to this line (see Fig. 2); the corresponding temperature is known as the pseudo-critical temperature. Density, thermal conductivity, and viscosity experience a significant decrease when crossing the Widom line (also Fig. 2). The property variations influence the heat transfer characteristics of supercritical fluids greatly. It is well known that density variations induce considerable buoyancy and acceleration forces, can lead to laminarization of the flow, which in turn leads to the deterioration of heat transfer [22]. Much literature has been devoted to addressing the heat transfer problem of supercritical fluids using both experimental methods (for instance [23]) and numerical methods (for instance [24]). This paper refers readers to recent reviews on this topic [25] instead of elaborating on every detail here.

The present work is aimed at finding novel trans-critical heat pump cycles that can provide heated air with a temperature of up to 200 °C. Four cycles with different working fluids are presented. The cycles' performance is evaluated using not only a 1st law analysis, but also by comparing the required condenser size, which in turn enables a detailed 2nd law analysis. The paper is organized as follows: In Section 2, the selection of suitable working fluids is presented. Section 3 describes the model of a trans-critical heat pump for the air drying process, including the first law analysis, the sizing of the gas cooler and the second law analysis. Corresponding results and discussions are then given in Section 4. Additionally, a comparison between the heat pump cycles based on the results of the first law & second law analysis as well as the sizing of the gas cooler is presented. Finally, the conclusions are summarized in Section 5.

2. Selection of working fluids

According to the Kigali Amendment to the Montreal Protocol [26], hydrofluorocarbon (HFC) refrigerants have to be gradually phased down because of their high global warming potential (GWP), for the sake of slowing down the trend of global warming. Furthermore, the usage of hydrochlorofluorocarbon (HCFC) and chlorofluorocarbon (CFC) was banned since 1994 because of their non-zero ozone depletion potential (ODP). Hence, this work limits the range of selection for working fluids to natural refrigerants, and newly developed low-GWP synthetic refrigerants like the hydrofluoroolefins (HFOs) and hydrofluoroethers (HFEs).

Reliable thermal stability to a temperature above 220 °C is another crucial criterion for screening out eligible working fluids. Normally, this criterion is an "all-pass" filter when designing heat pump cycles up to a maximum temperature below 100 °C, and thus is often neglected during the selection of working fluids [27]. However, it becomes a major concern when the maximum temperature is lifted up to 220 °C and it is therefore stressed here.

The critical temperature of the working fluids must not be too low compared to the aforementioned maximum temperature 220 °C. Otherwise, the heat pump cycle becomes a supercritical reversed Brayton cycle. Recent literature suggests that the COP of such cycles is low; see for instance the supercritical CO_2 heat pump for heating up molten salt proposed by GE, which has a COP of 1.3 [28]. Additionally, the maximum pressure in the reverse Brayton cycle would be very high, e.g., over 20 MPa when using supercritical CO_2. Hence, working fluids with critical temperatures lower than 85 °C are excluded as well. Working fluids with toxicity and flammability are commonly disregarded but they are not ruled out here.

Four refrigerants, listed in Table 1, were found to adhere to the aforementioned criteria: two HFO's, (R1233zd(E) and R1336mzz(Z)), one hydrocarbon (n-Butane), and one natural refrigerant (ammonia). Only n-butane and ammonia are flammable. Additionally, ammonia is also toxic. Their thermophysical properties are all extracted from the program REFPROP V10 [29]. The variation of their specific heat capacity, density, thermal conductivity, and viscosity with the temperature at two different reduced pressure levels was shown previously in Fig. 2.

3. Modeling methods

Fig. 3 illustrates the main components and flow streams in the model of an air-heating heat pump for an air-drying process. In this work, only heat pumps with internal heat exchangers are considered in order to avoid the complexity of advanced configurations, such as cascading cycles [35] or work recovery ejectors [36]. The modeled system consists of a gas cooler, a compressor, an evaporator, an expansion valve, and an internal heat exchanger. The internal heat exchanger is used to superheat the working fluid after the evaporator and thus enable lower source temperatures. By superheating the fluid, wet compression is avoided.

3.1. Assumptions for operation conditions of heat pump cycle

The heat pump cycle will be designed such that air with a mass flow rate of 10 kg/s can be heated to 200 °C. These criteria are typical for spray dryers used in the process industry [37]. It is assumed that the air is pre-heated to 80 °C using waste heat from the spray dryer [9,38]. Thus, the total power of the gas cooler is fixed to be $Q = 1.2$ [MW]. Other assumptions are listed below:

(i) The air dying process and the heat pump operate at a steady state;

(ii) Heat losses from different components and connected piping to the ambient environment are negligible;

(iii) The maximum temperature of the refrigerant reached at the outlet of the compressor is 220 °C;

(iv) The overall compression efficiency, defined as the product of mechanical and isentropic compressor efficiency, defined as

$$\eta_{comp} = \frac{h_{comp,o,isen} - h_{comp,i}}{h_{comp,o} - h_{comp,i}} \quad (1)$$

is conservatively chosen to be a relatively low number, 70%, since the thermodynamic cycles under consideration are novel;

(v) The temperature difference at the pinch-point at the high-temperature side of the internal heat exchanger is 10 °C;

(vi) The superheating of the refrigerant before the inlet of the compressor is provided by the internal heat exchanger;
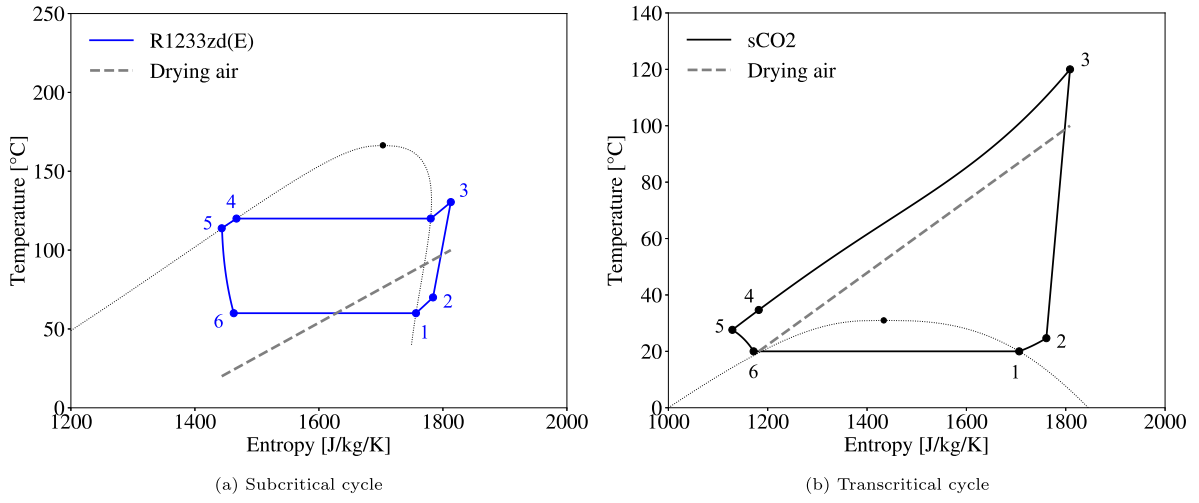
(a) Subcritical cycle

(b) Transcritical cycle

Fig. 1. Example heat pump cycles on T-s diagrams: 1 Outlet of the evaporator; 2 Inlet of the compressor; 3 Outlet of the compressor; 4 Outlet of the gas cooler; 5 Inlet of the expansion valve; 6 Outlet of the expansion valve.
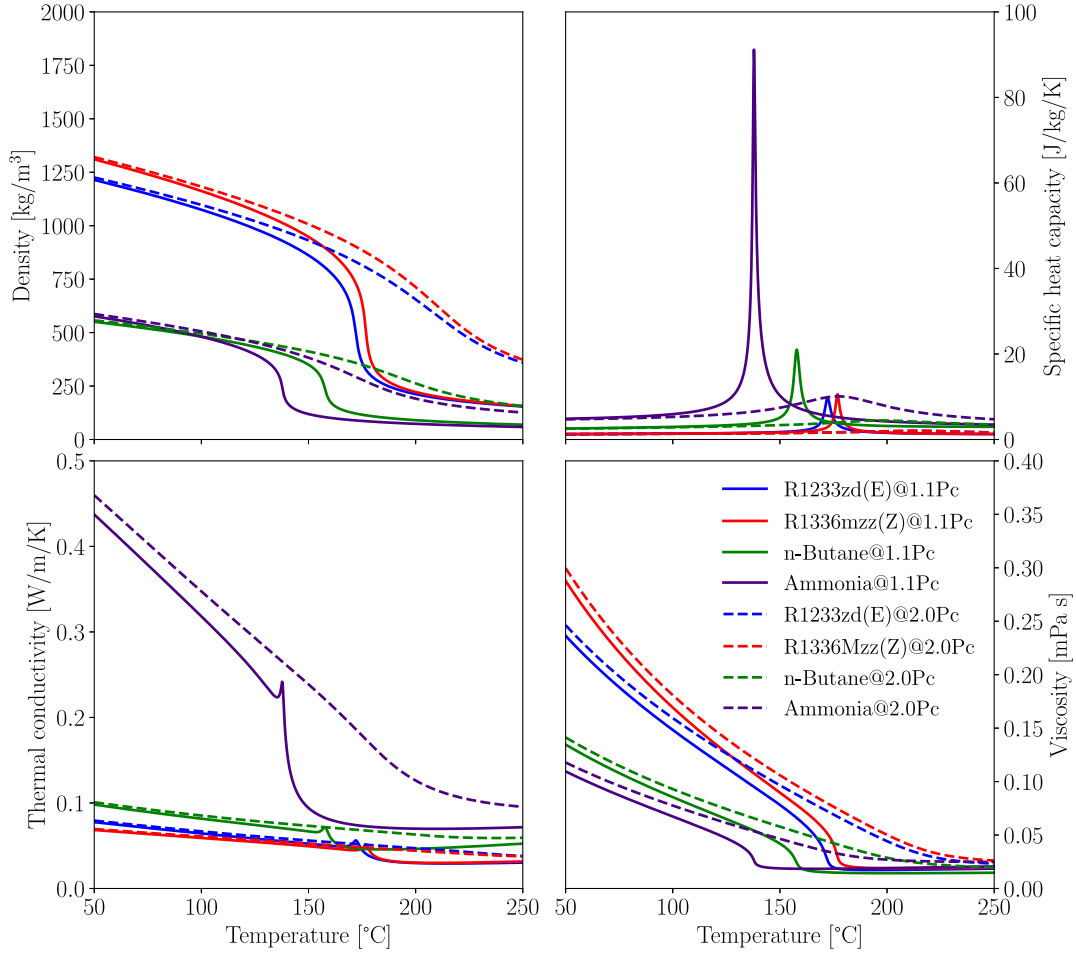

Fig. 2. Material property variation with the temperature at 1.1 times critical pressure (solid line) and 2.0 times critical pressure (dashed line) for different refrigerants.

(vii) An external extensive heat network [39] is assumed to be available as a heat source with a temperature of 88 °C. Thus, a 3 °C pinch is assumed for the evaporator. Hence, the evaporating temperature of the refrigerant is 85 °C;

(viii) The expansion process in the thermal expansion valve is isenthalpic.

3.2. First law analysis

The coefficient of performance, or COP, of the heat pump cycle is defined as the ratio of the heating power exchanged in the gas cooler, Q_{gc}, to the shaft power consumed by the compressor, W_{comp}[40]:

$$COP = \frac{Q_{gc}}{W_{comp}}. \tag{2}$$

Table 1

Properties of low-GWP refrigerants. Here, T_c, p_c, T_{limit} and P_{limit} stand for the critical temperature, pressure, thermal stability limit and pressure stability limit, respectively. Please note that different protocols exist for testing the thermal stability of working fluids [30].

Property name	Unit	R1233zd(E)	R1336mzz(Z)	n-Butane	Ammonia
Full name	–	1-Chloro-3,3,3-trifluoropropene	1,1,1,3,3-pentafluoro-propane	–	–
Formula	–	$C_3ClF_3H_2$	$C_4F_6H_2$	C_4H_10	NH_3
GWP	–	2	1	0.02	0
T_c	°C	166.5	171.4	152.0	132.4
p_c	bar	36	29	38	114
T_{limit}	°C	250 [31]	250 [32]	300 [33]	450 [34]
Flammability	–	Not flammable	Not flammable	Highly flammable	Slightly flammable
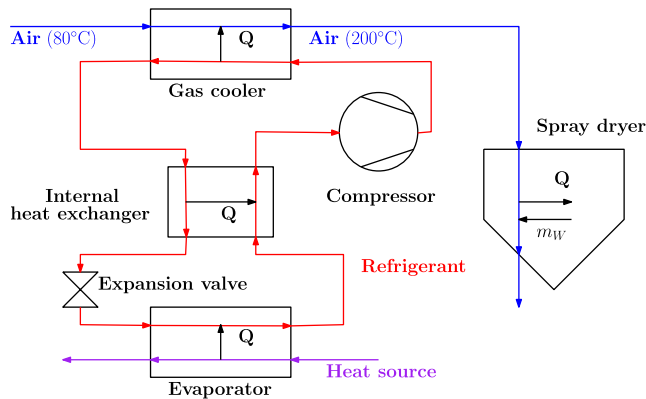
Fig. 3. Schematic of a heat pump for an air drying process.

Table 2

Specification of the shell-tube heat exchanger as the gas cooler.

Parameters	Unit	Values
Front head type	–	Bonnet
Shell type	–	Two-pass
Rear head type	–	U-tube bundle
Shell inner diameter	mm	692
Tube inner diameter	mm	26.6
Tube outer diameter	mm	33.4
Tube transverse pitch	mm	41.75
Tube arrangement	–	30° triangular
Number of tubes	–	204
Number of baffles	–	8

Even with the assumptions made in Section 3.1, the transcritical heat pump cycles are not yet fully determined. Following previous works on transcritical CO_2 heat pumps [41,42], the pressure ratio of the compressor will be regarded as an optimization parameter in Section 4. The optimization of the pressure ratio is performed such, that wet compression does not occur. Here "wet compression" refers to the circumstance in which the curve representing the compression process intersects with the liquid-vapor dome of the working fluid. Thus, wet compression can occur in working fluids whose dew line has a slope of $ds/dT > 0$ in the T-s diagram, even with superheating before the compressor inlet. As will be shown later, R1233zd(E), R1336mzz(Z), and n-Butane all possess this property. Hence, the avoidance of wet compression needs to be accounted for in optimizing the transcritical heat pump cycles using these working fluids.

3.3. Gas cooler sizing

As mentioned in Section 1, the sizing of the gas cooler in transcritical heat pump cycles needs to be handled carefully due to the effect of the pseudo-condensation of the refrigerants at supercritical pressure. When pseudo-condensation is significant (typically when p_r is close to unity), a pinch point may occur, which in turn can result in a very large gas cooler. The latter is generally an undesirable outcome as large gas coolers are costly and the space required for it might not be available on-site. The zero-dimensional condenser model which is commonly used in the calculation of subcritical heat pump cycles [43] is based on the overall mass and energy balance using the constant material properties of the working fluid at a representative temperature, such as the logarithmic mean temperature difference method [44]. This method cannot account for the heat transfer characteristics of supercritical fluids in the gas cooler, like the staged development characteristic along the axial direction [45], which is the result of large property variations in the vicinity of the pseudo-critical point, as was shown in Fig. 2. A one-dimensional gas cooler model which includes friction factor and heat transfer coefficient (HTC) correlations developed specifically for supercritical fluids that take their aforementioned traits into

account [46] is anticipated to alleviate such discrepancy and makes the sizing much more realistic. Such argument is also corroborated in [44] regarding the necessity of a one-dimensional model for the calculation of air-cooled finned tube heat exchangers used in a supercritical CO_2 Brayton power cycle. Since the geometry information, such as tube diameter etc., of the heat exchanger is needed in the calculation of a one-dimensional gas cooler model, sizing of a heat exchanger is necessary.

3.3.1. Sizing of a shell-tube heat exchanger as the gas cooler

The commercial software ASPEN® Exchanger Design & Rating V12.0 [47] is adopted in this work to perform the preliminary design of the gas cooler for the proposed cycles. The shell- and tube type heat exchanger is widely employed in the process industry; it is selected here for its simple stationary structure, robust working performance, high operating temperature and pressure tolerance, low purchase and maintenance cost. The air flowing in the shell is said to be a mixed stream, while the refrigerant flowing inside the tubes is said to be an unmixed stream [48]. The BMuU [49] TEMA standard type is chosen for this heat exchanger as a compromise between its occupied volume and the degree of complexity for its construction. The material of the tube bundles is selected to be stainless steel on account of the compatibility with ammonia. The dimension of the stainless steel pipe is set to be 1 inch with a thickness of 0.133 inch based on its pressure rating and the required mass flow rate of the heated air. At a temperature level of 260 °C, the maximum allowable stress is 13 114 kPa [50], which is enough to bear the most severe operation situation of the gas cooler for the proposed transcritical heat pump cycles. The main parameters of the sized shell-tube heat exchanger are summarized in Table 2 and are used in the calculation for the pressure drop and heat transfer characteristics of the gas cooler. The configuration of the tube bundles in the cross section of the sized shell-tube heat exchanger is illustrated below in Fig. 4.

To be able to use heat transfer correlations tailored to supercritical pressure (which are not available in ASPEN EDR), an in-house code is used to size the heat exchanger. In this code, a generalized version of the ϵ-NTU method [51] is used to calculate the heat transfer characteristics of the gas cooler.

With the geometry information of the cross-section for the sized shell-tube heat exchanger given in the previous section, the total length

Fig. 4. Cross section of the sized shell-tube heat exchanger.

Fig. 5. Flowchart of the one-dimensional calculation procedure for the gas cooler.

of the heat exchanger is changed iteratively to provide the required heating power. This iteration procedure is illustrated in Fig. 5. Since the thermodynamic states of the working fluid at the inlet and outlet of the gas cooler are given by the input conditions, the specific enthalpies at the inlet and outlet of the gas cooler are known. The gas cooler is then divided into 2000 segments with each one having an equal specific enthalpy interval. Based on energy conservation, the mass flow rate and the temperatures of the working fluid at the terminals of these segments can be obtained. After that, an initial length is assumed for the gas cooler, which is then equally divided into 2000 segments. Next comes the key step of this generalized version of the ϵ-NTU method. Once the effectiveness ϵ and the corresponding number of transfer units (NTU) of each segment are calculated, the length of that segment is updated according to

$$L_{gc,j} = NTU_j \frac{C_{min}}{2\pi D_{gc,tube,inner} U} \qquad (3)$$

where C_{min} denotes the minimum capacity rate, namely, the smaller one of $\dot{m}_r c_{p,r}$ and $\dot{m}_a c_{p,a}$. U denotes the overall heat transfer coefficient, which is a function of the heat transfer coefficients at the working fluid side, viz. the tube side, as well as the air side, viz., the shell side.

Currently, there exists no heat transfer correlation that is accurate for the selected fluids and their corresponding conditions. To obtain a reasonable estimate for the heat transfer coefficient of the refrigerant, the Yoon correlation [52], developed for predicting the heat transfer coefficient of cooling supercritical carbon dioxide in a horizontal tube with 7.73 mm inner diameter, is utilized for predicting the heat transfer coefficient at the tube side of the gas cooler. Its formulas for the jth segment are as follows:

$$Nu_{gc,r,j} = aRe_r^b Pr_r^c \left(\frac{\rho_{pc}}{\rho_r}\right)^n,$$
$$a = 0.14, b = 0.69, c = 0.66, n = 0 \quad \text{for} \quad T_r > T_{pc}$$
$$a = 0.013, b = 1.0, c = -0.05, n = 1.6 \quad \text{for} \quad T_r \leq T_{pc} \qquad (4)$$

Here Re_r denotes the Reynolds number of the refrigerant in the gas cooler, defined as

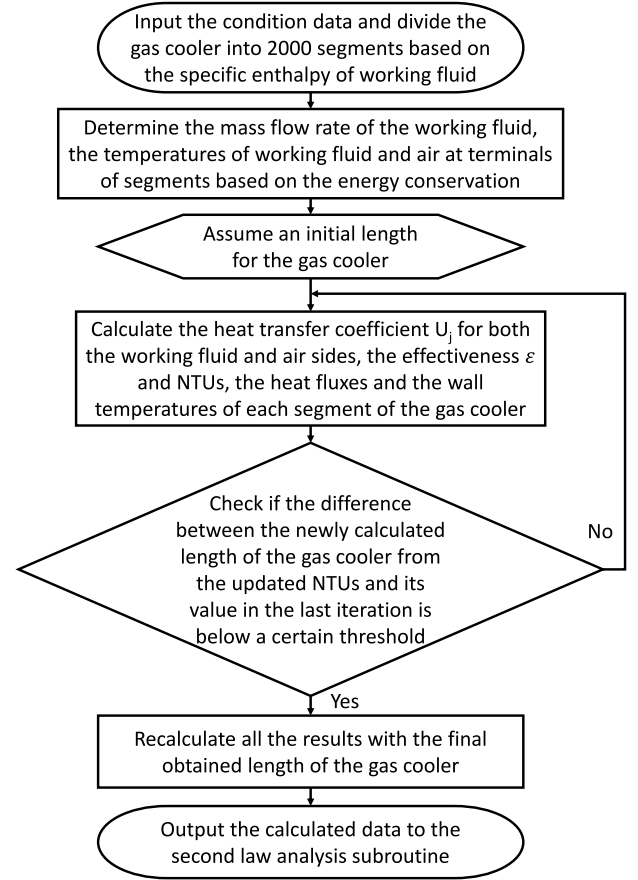$$Re_r = \frac{G_r D_{gc,tube,inner}}{\mu_r}, \qquad (5)$$

while Pr_r denotes the Prandtl number of the refrigerant, defined as

$$Pr_r = \frac{c_{pr}\mu_r}{\lambda_r}, \qquad (6)$$

The heat transfer at the shell side of the gas cooler is modeled in the form of free air streams flowing through staggered tube bundles. Thus, the Žukauskas correlation [53], reading

$$Nu_{gc,a,j} = ARe_{gc,a,max}^B Pr_a^{0.36} \left(\frac{Pr_a}{Pr_{aw}}\right)^{0.25}, \qquad (7)$$

is adopted to calculate the heat transfer coefficient at the shell side of jth segment. In Eq. (7) Pr_a and Pr_{aw} are the air Prandtl numbers evaluated at the bulk temperature and the wall temperature, respectively. A and B are constants whose values depend on $Re_{gc,a,max}$, as listed in Table 3. The Reynolds number $Re_{gc,a,max}$ is defined similarly as in Eq. (5) on the basis of the maximum air velocity $u_{gc,a,max}$. It occurs through the minimum flow area in the tube bank, which is evaluated as

$$u_{gc,a,max} = \frac{u_\infty (S_n/2)}{[(S_n/2)^2 + S_p^2]^{1/2} - D_{gc,tube,inner}}, \qquad (8)$$

where S_n and S_p are tube pitches along the directions perpendicular and parallel to the flow. u_∞ is the incoming free stream velocity of the air, which is evaluated as the velocity at the inlet channel of the shell.

After updating the lengths for 2000 segments of the gas cooler, the heat flux and wall temperature in each segment are updated. Then, the L^2-norm of the differences between the updated lengths and the lengths in the last iteration for 2000 segments are checked. The threshold for each length segment is chosen to be 0.005. If the threshold is not met, the effectiveness and NTU of each segment are recalculated.

The method to determine the length of the gas cooler was validated against a finite difference solution of a heat exchanger in which supercritical CO_2 is cooled by water [21]. The details of this case as well as the validation results of the current methods can be found in Appendix A.

3.3.2. Pressure drop calculation

Calculation of the pressure drop for the gas cooler is also necessary for verifying the sizing of the shell-tube heat exchanger. Fang, et al. [54] have developed a correlation specifically for the prediction of the pressure drop of a supercritical fluid in the gas cooler. The total pressure drop is calculated as the sum of the pressure drop in each jth segment:

$$\Delta P_{gc,r} = \sum_{j=1}^{N} \left[\frac{G_r^2}{\rho_r} \left(f_{gc,r,j} \frac{L_{gc,j}}{D_{gc,tube,inner}} + 1.2 \right) \right], \tag{9}$$

where $f_{gc,r}$ denotes the Filonenko friction factor,

$$f_{gc,r,j} = \frac{1}{[0.79 \ln(\text{Re}_{gc,r,j} - 1.64)]^2}. \tag{10}$$

As mentioned in Section 3.2, the flow of air at the shell side of the gas cooler is modeled in the form of free air streams passing through staggered tube bundles. So the pressure drop of air at the shell side can be calculated as,

$$\Delta P_{gc,a} = 2 f_{gc,a} u_{gc,a,max}^2 \rho_a n_{row} \left(\frac{\mu_{aw}}{\mu_a} \right)^{0.14}, \tag{11}$$

where n_{row} denotes the number of transverse rows of tube bundles that the air stream passes, and $f_{gc,a}$ denotes the Jakob friction factor [55], which is evaluated as

$$f_{gc,a} = \left(0.25 + \frac{0.118}{[(S_n - D_{gc,tube,inner})]^{1.08}} \right) Re_{gc,a,max}^{-0.15}. \tag{12}$$

3.4. Second law analysis

Following the sizing of the gas cooler, the pressure drop and the exact heat transfer rates at each temperature level can now be calculated, both of which are necessary for the second law analysis. Second law analysis gives the irreversibility, or entropy production, generated per components of the thermodynamic system [56] and is generally considered to complement the first law analysis. Hereafter, the methods to calculate the irreversibility in each component are presented. Moreover, a relation between the COP (see Section 3.2) and the irreversibility generation is used as a means of validating the second law analysis.

3.4.1. Irreversibility calculation

The total irreversibility generated in the gas cooler I_{ihx} is calculated as

$$I_{gc} = I_{gc,\Delta T} + I_{gc,\Delta P}, \tag{13}$$

where $I_{gc,\Delta T}$ is the irreversibility generated due to the temperature difference between the working fluid and the air, calculated as

$$I_{gc,\Delta T} = T_{ev,hs} \sum_{j=1}^{N} \left(\frac{Q_{gc,j}}{T_{gc,air,j}} - \frac{Q_{gc,j}}{T_{gc,r,j}} \right), \tag{14}$$

and $I_{gc,\Delta P}$ is the irreversibility generated due to the pressure drop of the refrigerant and the air in the gas cooler, calculated as

$$I_{gc,\Delta P} = \frac{\dot{m}_r}{\rho_r} \Delta P_{gc,r} + \frac{\dot{m}_a}{\rho_a} \Delta P_{gc,a}. \tag{15}$$

Irreversibility terms relevant to other components of transcritical heat pump cycles are kept the same as in Alefeld's original framework and their calculation equations are given as follows: The irreversibility generated in the evaporator I_{ev} is calculated as

$$I_{ev} = I_{ev,\Delta T} + I_{ev,\Delta P}, \tag{16}$$

where $I_{ev,\Delta T}$ is the irreversibility generated due to the temperature difference between the refrigerant and the heat source, calculated as

$$I_{ev,\Delta T} = T_{ev,hs} \left(\frac{Q_{ev}}{T_{ev,r}} - \frac{Q_{ev}}{T_{ev,hs}} \right), \tag{17}$$

and $I_{ev,\Delta P}$ is the irreversibility generated due to the pressure drop of the refrigerant in the evaporator, calculated as

$$I_{ev,\Delta P} = \frac{\dot{m}_r}{\rho_r} \Delta P_{ev,r}. \tag{18}$$

Detailed calculation methods for these quantities can be found in Appendix C. The irreversibility generated in the internal heat exchanger I_{ihx} is calculated as

$$I_{ihx} = T_{ev,hs}(\Delta s_{ihx,c} - \Delta s_{ihx,h}), \tag{19}$$

where $\Delta s_{ihx,c}$ and $\Delta s_{ihx,h}$ denotes the entropy difference of the refrigerant between the inlet and outlet at the cold side and the hot side of the internal heat exchanger. The irreversibility generated in the expansion valve I_{comp} is calculated as

$$I_{comp} = \dot{m}_r T_{ev,hs} \Delta s_{comp}, \tag{20}$$

where Δs_{comp} denotes the entropy difference between the inlet and outlet of the compressor. The irreversibility generated in the expansion valve I_{exp} is calculated as

$$I_{exp} = \dot{m}_r T_{ev,hs} \Delta s_{exp}, \tag{21}$$

where Δs_{exp} denotes the entropy difference between the inlet and outlet of the expansion valve.

Finally, to put cycle losses in perspective, the second law efficiency can be calculated:

$$\eta = \frac{COP}{COP_{Lorenz}}, \tag{22}$$

where, COP_{Lorenz} is defined as

$$COP_{Lorenz} = \frac{\overline{T}_{gc,air}}{\overline{T}_{gc,air} - T_{ev,hs}} \tag{23}$$

where $\overline{T}_{gc,air}$ denotes the entropic average of the air temperature in the gas cooler [57], i.e.,

$$\overline{T}_{gc,air} = \frac{q_{gc}}{s_{gc,air,o} - s_{gc,air,i}}. \tag{24}$$

Here q_{gc} denotes the specific heating power exchanged in the gas cooler, which is obtained by dividing the heating power Q_{gc} with the mass flow rate of the refrigerant $\dot{m}_r$.

3.4.2. Relation between first- and second law analysis

Alefeld's framework [57] is adopted to connect the irreversibility to the first law results in Section 3.2. This framework connects the second law to the first law by establishing a relation between the coefficient of performance and the generated irreversibility. This relation will be used as a validation of the second law analysis calculations later. Unlike exergy analysis [40], this relation does not require the introduction of another parameter in the form of a reference temperature. Instead, the
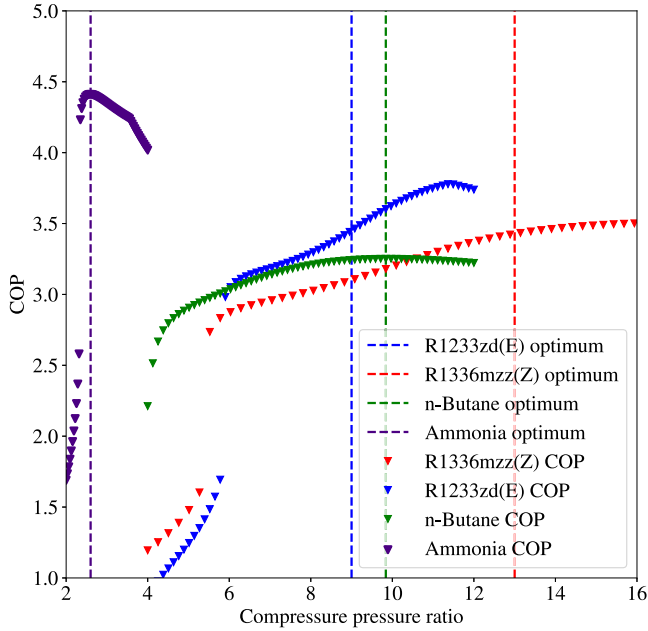
Fig. 6. COP vs. pressure ratio of the compressor for different transcritical heat pump cycles. For ammonia and n-Butane, the vertical lines represent optimum points. Note that for the optima of R1233zd(E) and R1336mzz(Z), wet compression occurs. Therefore, a pressure ratio with high COP, but without wet-compression is chosen for these fluids; these points have also been indicated by a vertical line.

reference temperature follows naturally from the consideration of the first and second laws together. The relationship is written as:

$$\text{COP} = \frac{\frac{\overline{T}_{gc,air}}{\overline{T}_{gc,air}-T_{ev,hs}}}{1+\frac{T_{ev,hs}\overline{T}_{gc,air}}{\overline{T}_{gc,air}-T_{ev,hs}}\frac{\sum_{i=1}^{n}\Delta s_i}{q_{gc}}}, \tag{25}$$

Originally, the entropy production Δs was separated into a desuperheating part and a condensing part. In the current work, the condenser is divided into $n = 2000$ segments. Using the results of the one-dimensional calculation for the gas cooler, the irreversibility generation in each segment is easily calculated.

4. Results and discussions

The calculation results based on the modeling methods described in Section 3 are presented here in the same order as the model was presented in Section 3.

4.1. First law analysis results

Fig. 6 shows the calculated COP versus the compressor pressure ratio for the four selected working fluids. All heat pump cycles display a strong increase of COP with compression ratio. For ammonia, R1233zd(E) and n-Butane, an optimum is visible as well. This trend is very similar to results that were reported by [58]. Special attention must be paid to R1233zd(E) and R1336mzz(Z). For these fluids, wet compression occurs for the pressure ratios that correspond to the highest COPs, as in those cases the compression line would intersect with the dew line of the working fluids. By superheating the refrigerant to a higher temperature in the internal heat exchanger and simultaneously decreasing the pressure ratio (to comply with assumption (iii) in Section 3.1), wet compression is avoided entirely. Consequently, the COP decreases from 3.8 to 3.6 for R1233zd(E) and decreases from 3.6 and 3.4 for and R1336mzz(Z).

The T-s diagrams of the proposed transcritical heat pump cycles with different working fluids are plotted in Fig. 7. It is clear that

wet compression does not occur in any of the cases. Furthermore, the R1233zd(E), R1336mzz(Z), and n-Butane transcritical heat pump cycles have similar shapes. In the ammonia case, the isobaric cooling process is completely different. The latter is an indicator of the strong pseudo-condensation phenomenon occurring in the gas cooler [21], which is much less significant in the other cycles. This difference is mainly due to the lower reduced pressure of ammonia, $p_r \approx 1.1$, compared to the reduced pressure of R1233zd(E), R1336mzz(Z), and n-Butane, which is close to 2.0, in the gas cooler. As is clear from Fig. 2, the variation of material properties for working fluids with reduced pressure close to 2.0 is not as strong as it is at a reduced pressure of 1.1. Consequently, it is likely that the pseudo-condensation phenomenon affects the design of the gas cooler more significantly in the ammonia case than in the other cases.

4.2. Gas cooler sizing results

Given the results of the optimal cycles for the four different fluids, the size and performance of the gas coolers may now be analyzed. Before doing so, it should be noted that for the optimal ammonia cycle presented in Fig. 7, it is impossible to heat the air from 80 °C to 200 °C. In Fig. 8(a), the temperature glide of the optimal ammonia cycle is shown. If the air is to be heated to 200 °C, it becomes immediately clear that the air inlet temperature must be significantly lower than 80 °C, i.e. 50 °C, as a result of the pinch point. The latter condition violates the assumptions mentioned in Section 3. To make a fair comparison between the four refrigerants, the maximum temperature of the ammonia heat pump cycle is increased to 235 °C, to enable an air inlet temperature of 80 °C; see Fig. 8(b). By raising the temperature slightly, the compression ratio changes from 2.60 to 2.92. Consequently, the COP of the ammonia cycle decreases from 4.41 to 4.04.

The sizing of the gas coolers is affected in two different ways; (1) the variation of the specific heat capacity affects the sizing directly due to the occurrence of the previously discussed pinch-point, while (2) the combination of varying thermophysical properties (Fig. 2) affects the magnitude of the heat transfer coefficient significantly. Therefore, it is interesting to investigate the sizing of the gas coolers in detail. The axial distribution of the air temperature, refrigerant temperature, and the wall temperatures are plotted versus the axial length of the gas cooler in Fig. 9. It can be seen that the axial temperature distributions for the R1233zd(E), R1336mzz(Z) and n-Butane cases exhibit similar patterns, while the axial temperature distribution for the ammonia case is clearly different near the pseudo-critical temperature of the refrigerant. Correspondingly, the heat flux distribution curves plotted in Fig. 10 also exhibit such distinction between the R1233zd(E), R1336mzz(Z), n-Butane cases and the ammonia case.

In the first three cases, the heat flux increases first and then decreases with the bulk enthalpy of the refrigerant. In the ammonia case, the heat flux decreases drastically after passing the pseudo-critical point. At first, it is logical to attribute the decrease of the heat flux to the decreasing temperature difference between air and refrigerant. However, the temperature difference does not explain the initial increase in heat flux. The latter must be explained by investigating the local heat transfer coefficient, which is plotted in Fig. 11. The air convective heat transfer coefficients are very similar in all cases. In contrast, the refrigerant convective heat transfer coefficients are remarkably different. The heat transfer coefficients of n-Butane and R1336mzz(Z) increase with refrigerant bulk temperature and surpass the air heat transfer coefficient just beyond the point when $T_b = 180$ ^{o}C. However, the heat transfer coefficients of R1233zd(E) and ammonia show a local maximum close to the point where the bulk temperature is equal to the pseudo-critical temperature. The difference in magnitude of the local maxima can be explained as follows. For the R1233zd(E) case, the operating pressure in the gas cooler is nearly 2.0 times the critical pressure, while in the ammonia case, the pressure is only 1.1
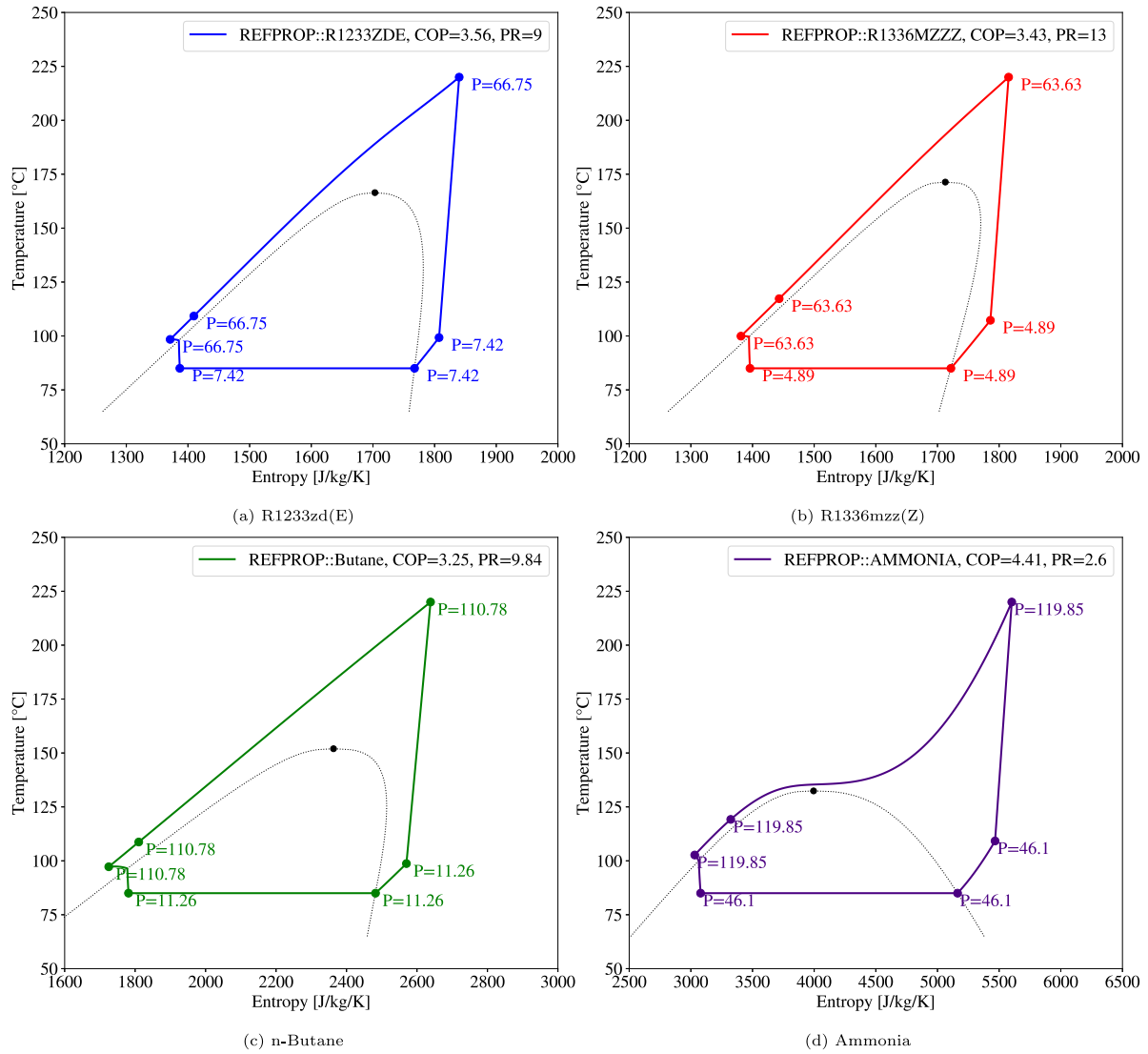
Fig. 7. T-s diagrams for the transcritical heat pump cycles with different working fluids.
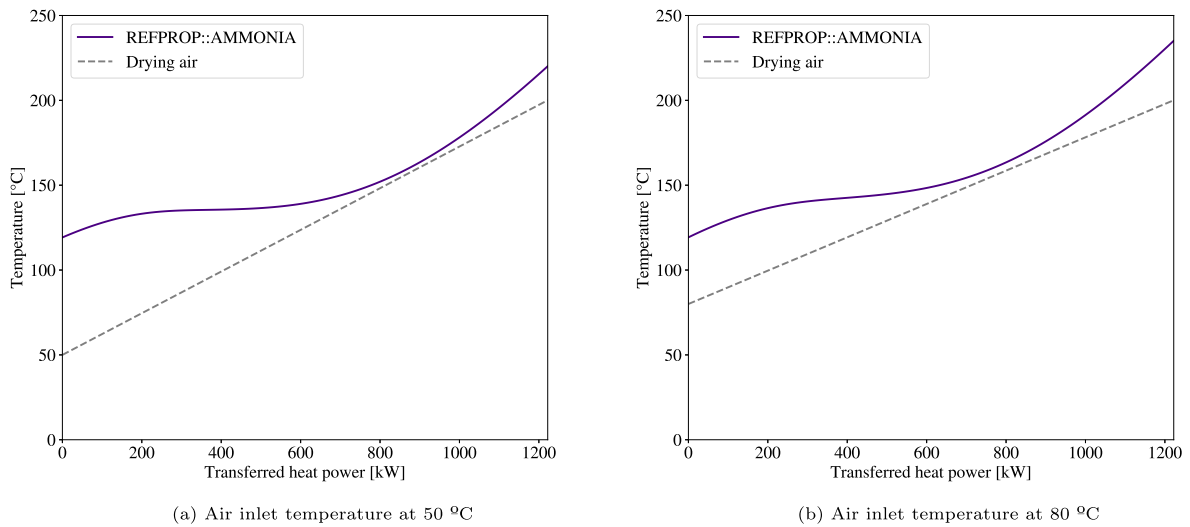

Fig. 8. T-q diagram of the gas cooler in the ammonia heat pump cycles. (a) the gas cooler in the optimal cycle. (b) the gas cooler in the adjusted ammonia cycle.
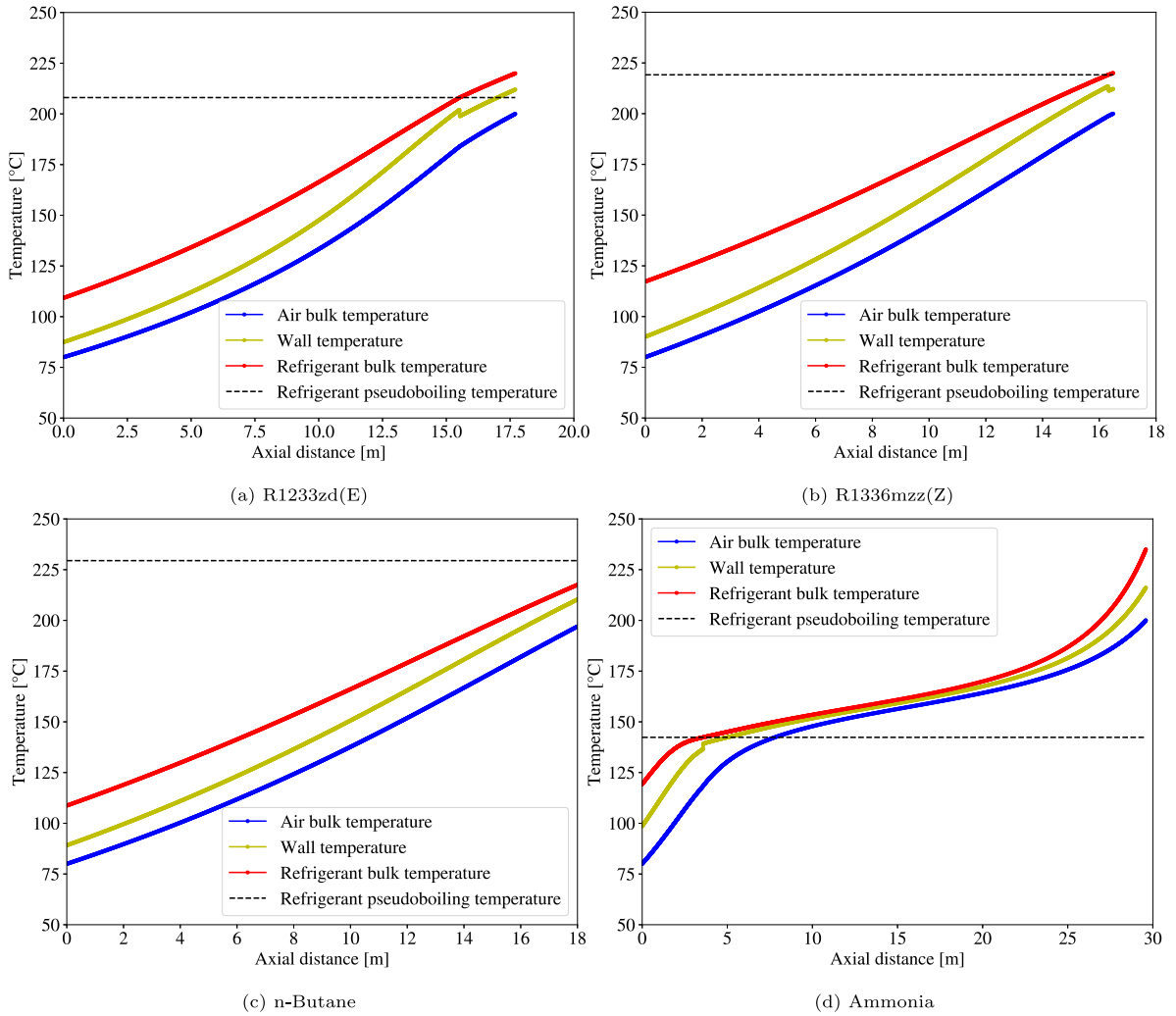
(a) R1233zd(E)

(b) R1336mzz(Z)

(c) n-Butane

(d) Ammonia

Fig. 9. Axial temperature distribution in the gas cooler. The dashed line indicates the pseudocritical temperature.

times the critical pressure. The latter means that the pseudo-boiling phenomenon is much stronger for the ammonia cycle.

Note that the discontinuity in the heat transfer coefficient is a result of the formulation of the Yoon correlation close to the pseudocritical point [52]. As a result, a similar discontinuity is present in the heat flux and temperature profiles in Fig. 10(a), (b) and Fig. 11(a), (b). As the heat transfer coefficient for the refrigerant suddenly drops, the heat transfer coefficient for the air becomes more dominant. Consequently, the wall temperature shifts towards the air temperature.

In conclusion, the heat flux profiles are clearly the result of not only the temperature difference between refrigerant and air but also the local heat transfer coefficient. Note that in the ammonia case, the minimal temperature difference requires the gas cooler to be more than twice as long as the gas coolers in the other cases. It should be mentioned here that the usage of different heat transfer correlations results in different heat exchanger lengths. Using six different correlations, it was found for instance that the required length of the gas cooler in the ammonia case varied from 20 to 55 m. These results are shown in detail in Appendix B.

Table 4 shows the results of the pressure drop calculation for the gas cooler for the four working fluids. The shell side pressure drop is much larger than the tube side. Note that spray dryers usually require compressed air as their input [59]. The ratios of pressure drop for all working fluids to their inlet pressure at the gas cooler are all below 0.5%, which justifies the implicit assumption in the first law analysis for the developed transcritical heat pump cycle that the influence of

Table 4
Pressure drop in the gas cooler.

Working fluid	ΔP at the tube side [Pa]	ΔP at the shell side [Pa]
R1233zd(E)	21 409	63 388
R1336mzz(Z)	22 930	64 240
n-Butane	11 916	64 275
Ammonia	5199	64 338

pressure drop in the gas cooler on material properties of the working fluids are negligible.

4.3. Second law analysis results

The comparison between the calculated COP from the first thermodynamic law analysis results in Section 3.2 and the second thermodynamic law analysis calculated with Eq. (25) is listed in Table 5. The relative error, which is calculated as $(COP_2 - COP_1)/COP_1$, is smaller than 0.5%. This result not only validates efforts in extending Eq. (25) to transcritical heat pump cycles but also indicates that the irreversibility calculation procedure is correct.

The fractions of irreversibility production in different components of the transcritical heat pump cycles calculated with Eq. (13) to Eq. (21), are demonstrated in Fig. 12. The total amount of entropy production is inversely correlated with the COP of each cycle. The same can be said for the second law efficiency, defined in Section 3.4. For R1233zd(E),
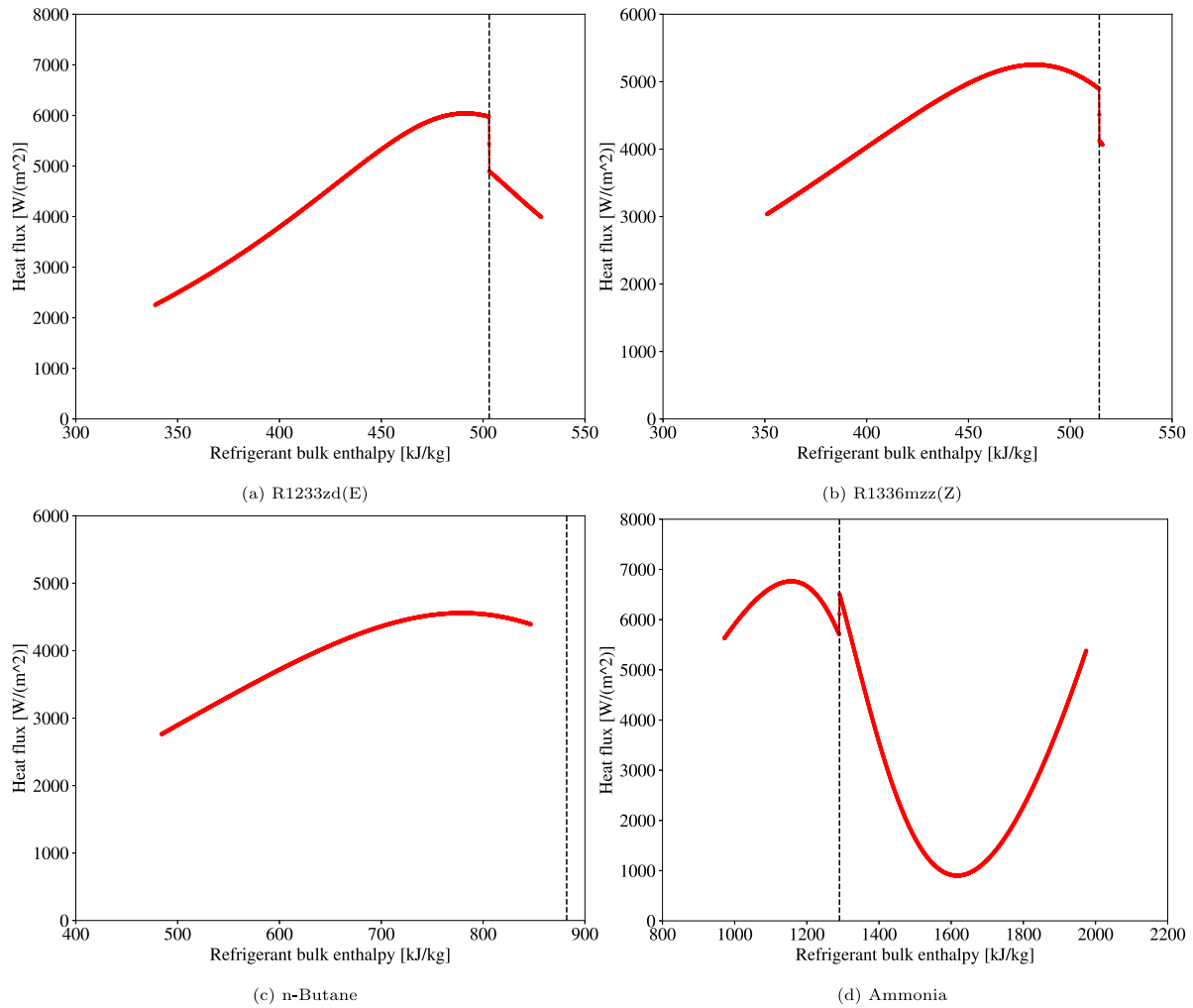
(a) R1233zd(E)

(b) R1336mzz(Z)

(c) n-Butane

(d) Ammonia

Fig. 10. Heat flux distribution in the gas cooler.

Table 5
Comparison of COPs calculated from the first law analysis and second law analysis.

Working fluids	COP with Eq. (2)	COP with Eq. (25)	Relative error
R1233zd(E)	3.56	3.57	0.25%
R1336mzz(Z)	3.43	3.44	0.24%
n-Butane	3.25	3.26	0.23%
Ammonia	4.41	4.42	0.31%

R1336mzz(Z), n-Butane and Ammonia, the second law efficiency is 43%, 41%, 39% and 48%. It is found that the irreversibility produced in the compressor takes the largest share, closely followed by the irreversibility produced in the gas cooler. The irreversibility produced in the evaporator and the internal heat exchanger merely occupies a share smaller than 5%, owing to the very small temperature differences between the refrigerant and the heat source in the evaporator, and the two streams of refrigerants in the internal heat exchanger. The irreversibility production in the compressor and recuperator in the ammonia cycle takes a larger share compared to other cycles. This difference is likely the result of the larger maximum temperature at the compressor outlet, 235 °C, the necessity of which was explained in Section 4.2. Furthermore, the Butane heat pump cycle has much more irreversibility production in its expansion valve than the other cycles. This result follows from the large entropy difference between the high pressure and low pressure side of the valve, as can be seen in Fig. 7c. Finally, the entropy generation in the gas coolers of the R1233zd(E)

and R1336mzz(Z) is larger than it is in the other cycles, because the temperature difference is relatively large as well.

4.4. Comparing cycles

To summarize the calculated results in a qualitative manner, Table 6 compares the four transcritical heat pump cycles based on four criteria:

- COP and second law efficiency, which are related to energy saving and carbon emissions.
- Maximum pressure, which is related to the material requirement and the safety concern for the compressor, expansion valve and the gas cooler.
- Compression pressure ratio, which is related to the isentropic efficiency and the cost of the compressor.
- Gas cooler length, which is related to the investment cost and occupied space taken by the gas cooler.

It can be seen that the R1233zd(E) cycle achieves a balanced score in all criteria, while the other cycles do not perform well in at least perform one criterion. Hence, the R1233zd(E) transcritical heat pump cycle is judged to be the most promising cycle for the purpose of heating air up to 200 °C for spray drying processes.

5. Conclusions

In this paper, high-temperature transcritical heat pump cycles with internal heat exchangers using low-GWP working fluids, R1233zd(E),
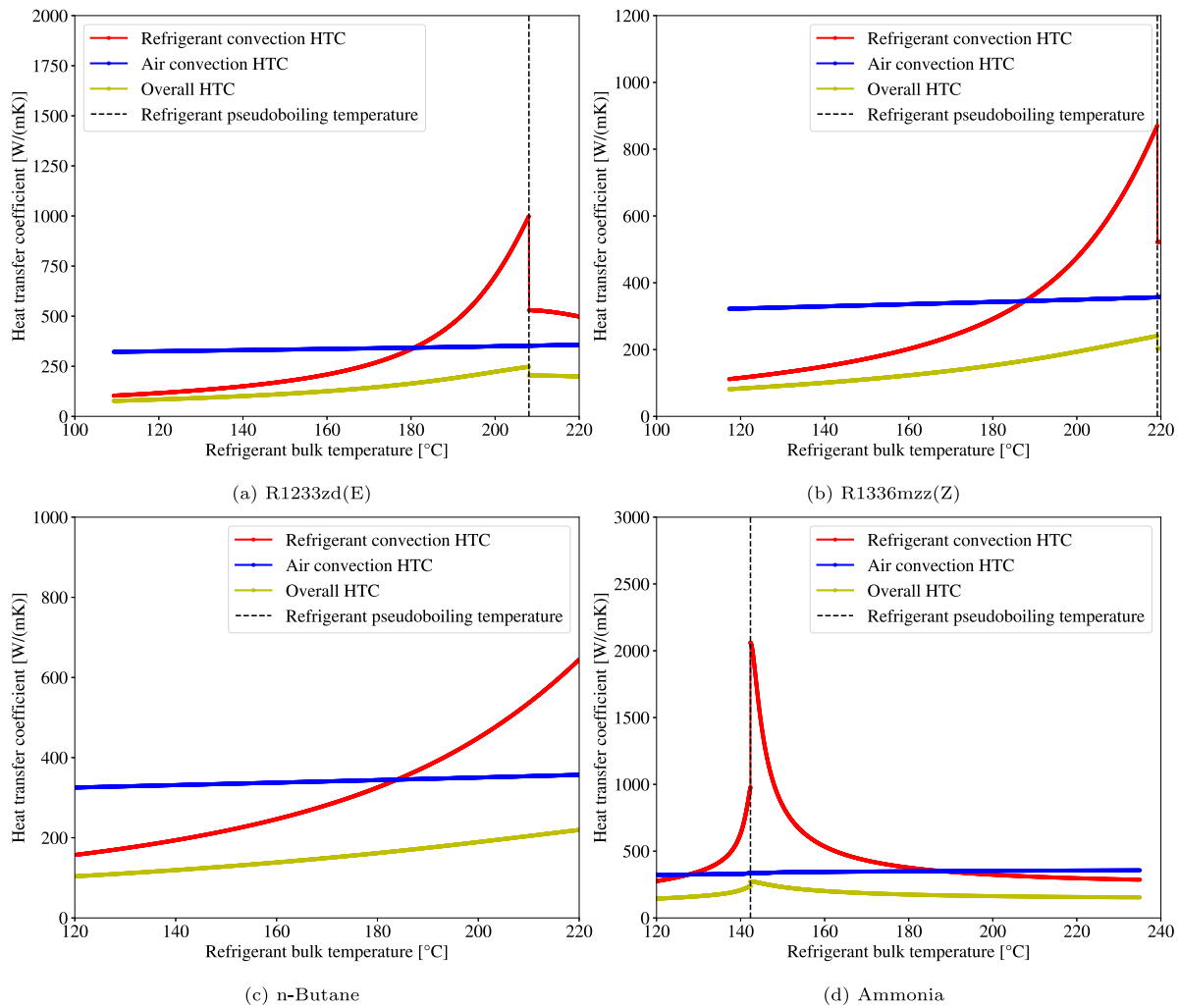
(a) R1233zd(E)

(b) R1336mzz(Z)

(c) n-Butane

(d) Ammonia

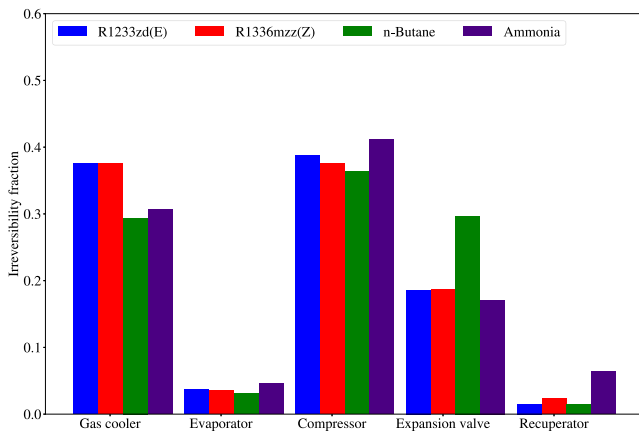**Fig. 11.** Axial HTC variation in the gas cooler.

Fig. 12. Fractions of irreversibility production in different components of the heat pump systems. The irreversibility for each cycle is $2.0 \cdot 10^5$, $2.1 \cdot 10^5$, $2.4 \cdot 10^5$, and $1.6 \cdot 10^5$ W for the R1233zd(E), R1336mzz(Z), n-Butane and ammonia heat pump cycles, respectively.

R1336mzz(Z), n-Butane and Ammonia are proposed for the purpose of heating air from 80 to 200 °C in spray drying applications. The mass flow rate of the drying air was set to 10 kg/s. In addition to performing first- and second law analyses, the gas cooler was sized in

Table 6

Comparison among transcritical heat pump cycles based on different criteria.

Working fluids	R1233zd(E)	R1336mzz(Z)	n-Butane	Ammonia
COP, η	+	+	−	++
Maximum pressure	+	++	+	−
Compression pressure ratio	+	−	+	++
Gas cooler length	+	+	++	−

Here "++" denotes most favorable, "+" denotes favorable, "−" denotes less favorable.

all cases, while accounting for the rapid variation of the thermophysical properties of the refrigerants at supercritical pressure. Following first- and second law analyses and the sizing of the gas cooler, the main conclusions are formulated as follows:

1. The optimal pressure ratios of the compressor for maximizing the COP of the transcritical heat pump cycles without incurring wet compression are approximately 9, 13, 9.8 and 2.6 for R1233zd(E), R1336mzz(Z), n-Butane and ammonia, respectively, while the pressure inside the gas cooler is 66.8, 63.6, 110.8 and 119.9 bars. The corresponding COP for these cycles is 3.6, 3.4, 3.3, 4.0, respectively.

2. As a result of the strong influence of pseudo-condensation in the ammonia case, a pinch-point occurs, which leads to the length of its gas cooler being twice as large as the gas coolers in the other cases.
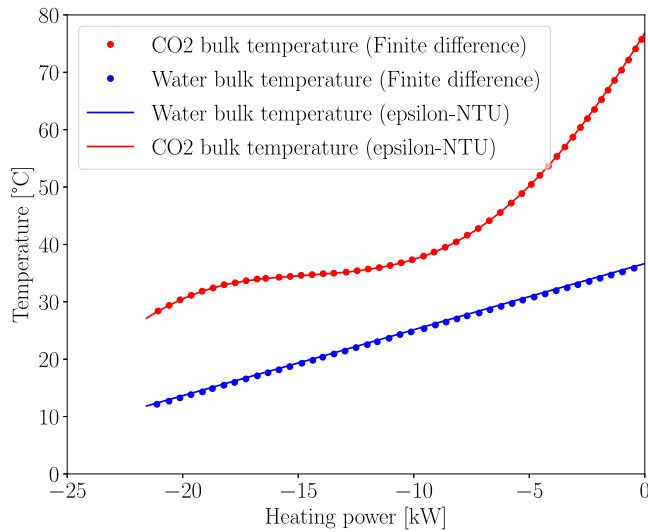
Fig. 13. Axial temperature distribution in the heat exchanger of the test case. Lines represent the current code, while the symbols represent the finite difference solution.

3. The compressor produces the largest fraction of irreversibility for all four cycles, closely followed by the gas cooler. Future optimization of the transcritical heat pump systems should be mainly targeted on these two components.

4. Even though the ammonia cycle has the most favorable pressure ratio of all the work fluids considered, it is also the most toxic, operates at the highest pressure and requires the largest gas cooler. Hence, the transcritical heat pump cycle using R1233zd(E) is considered the most promising candidate to provide heating in spray-drying applications, as it has the second largest COP (3.6), operates at a maximum pressure of only 67 bar, is non-flammable and does not require an excessively large gas cooler.

CRediT authorship contribution statement

An Zhao: Writing – original draft, Visualization, Validation, Software, Methodology, Investigation, Formal analysis, Data curation. **Rene Pecnik:** Writing – review & editing, Visualization, Supervision, Software, Methodology, Funding acquisition, Formal analysis, Conceptualization. **Jurriaan W.R. Peeters:** Writing – review & editing, Validation, Supervision, Project administration, Methodology, Funding acquisition, Formal analysis, Conceptualization.

Declaration of competing interest

The authors declare that they have no known competing financial interests or personal relationships that could have appeared to influence the work reported in this paper.

Data availability

Data will be made available on request.

Acknowledgments

Table A.7
Conditions for the 1D calculation and analytical solution of the heat exchanger in the test case.

Fluid	Parameters	Unit	Values
Water	$\dot{m}_c$	kg/s	0.208
	$p_{gc,in,c}$	bar	1
	$T_{gc,in,c}$	°C	11.85
Carbon dioxide	m_h	kg/s	0.1
	$P_{gc,in,h}$	bar	80
	$T_{gc,in,h}$	°C	76.85
	$T_{gc,out,h}$	°C	27.15

Appendix A. Comparison of results between the one-dimensional heat exchanger calculation and the finite difference analytical solution for a test case

In order to verify the code for the one-dimensional calculation of the gas cooler, an extra test case has been run for a heat exchanger for which a validated finite difference solution is available [21]. It is designed to transfer heat from supercritical carbon dioxide to water, whose operation conditions can be found in Table A.7. For the geometry schematic of the heat exchanger cross section, the reader is kindly referred to Fig. 4 in [21]. The heat exchanger has six tubes where the supercritical carbon dioxide stream flows in. The inner diameter of each tube is 5 mm while the outer diameter is 6.6 mm. The water stream flows in the shell side, whose inner diameter is 25.4 mm. The total length of the heat exchanger is set to be 3 m, while the total heat transfer coefficient between the supercritical carbon dioxide and the water is set to be constant at 3000 W/(m²K). The finite difference solution is based on the following transport equations,

$$
\begin{aligned}
C_{p,h}\frac{dT_h}{dz} - \frac{d}{dz}\left(k_h\frac{T_h}{dx}\right) - U_t P_t(T_h - T_c) = 0, \\
C_{p,c}\frac{dT_c}{dz} - \frac{d}{dz}\left(k_c\frac{T_c}{dx}\right) - U_t P_t(T_h - T_c) = 0.
\end{aligned}
\tag{26}
$$

Here, the heat capacity of the water at constant pressure is assumed to be equal to 4180 J/(kg K), while the specific heat capacity of the carbon dioxide varies with temperature.

The same case is recreated while using the generalized version of the ϵ-NTU method model previously described in, with the exception of the total length of the heat exchanger, which is now an unknown that needs to be solved. The calculated total length of the heat exchanger turns out to be 3.00038 m, which is deemed to be consistent with the finite difference solution. The obtained axial temperature distribution in the heat exchanger is plotted in Fig. 13 and shows the exact shape as in the finite difference solution, thus validating the methods outline in Section 3.3.

Appendix B. Comparison of different heat transfer coefficient correlations for supercritical fluids in the one-dimensional calculation of the gas cooler

As mentioned in Section 3.2 of the main text, the one-dimensional calculation for the heat transfer characteristics of the gas cooler is supposed to be sensitive to the working fluid side HTC. Hence, the selection of the supercritical heat transfer correlation affects the first law analysis results a lot and is worth carefully addressing. Nevertheless, some previous supercritical heat transfer correlations developed for heating processes cannot be directly applied in the cooling processes without any revision. For instance, the Yamagata correlation [60] switches between different equations for determining the values of parameters in the correlation via comparing $\frac{T_{pb}-T_r}{T_{rw}-T_r}$ with constants 0 and 1, but obviously the denominator of this term has different symbols in the

heating or cooling situation. Therefore, the application of these correlations in calculating the heat transfer at the working fluid side in the gas cooler is invalidated. After a detailed survey of the literature related to supercritical heat transfer and excluding those ruled-out ones, six correlations stand out as viable options. Their targeted scenarios are summarized as follows, while their full equations, applicable pressure levels, heat/mass flux ranges are not repeated here and the readers are referred to the original publications:

(1) The Swenson correlation [61] developed for predicting the HTC of heating supercritical water flowing upwards in a vertical tube with 9.4 mm inner diameter. Its formula is as follows:

$$Nu_{gc,rw} = 0.00459 Re_{rw}^{0.923} \overline{Pr}_{rw}^{0.613} (\frac{\mu_r}{\mu_{rw}})^{0.231}, \tag{27}$$

where $Nu_{gc,rw}$ denotes the Nusselt number of the refrigerant in the gas cooler defined at the wall temperature, and Re_{rw} denotes the Reynolds number of the refrigerant in the gas cooler at the wall temperature, defined as

$$Re_{rw} = \frac{G_r D_{gc,tube,inner}}{\mu_{rw}}. \tag{28}$$

Moreover, here $\overline{Pr}_{rw}$ denotes the average refrigerant Prandtl number defined at the wall temperature,

$$\overline{Pr}_{rw} = \frac{\bar{c}_{pr} \mu_{rw}}{\lambda_{rw}}, \tag{29}$$

where $\bar{c}_{ph}$ denotes the average specific heat integrated between the bulk fluid and the wall temperature,

$$\bar{c}_{ph} = \frac{h_r - h_{rw}}{T_r - T_{rw}} \tag{30}$$

(2) The Petukhov correlation [62] developed for predicting the HTC of heating different supercritical fluids flowing towards different directions in tubes with different inner diameters. Its formulas are as follows:

$$Nu_{gc,r} = \frac{(\xi/8) Re_r \overline{Pr}_r}{1 + 900/Re_r + 12.7\sqrt{(\xi/8)}(\overline{Pr}_r^{2/3} - 1)}, \tag{31}$$

where ξ is calculated as

$$\xi = \frac{(\rho_{hw}/\rho_h)^{0.4}(\mu_{hw}/\mu_h)^{0.2}}{[1.82 \log_{10}(Re_h) - 1.64]^2}. \tag{32}$$

Here $\overline{Pr}_r$ denotes the average refrigerant Prandtl number defined at the bulk temperature,

$$\overline{Pr}_r = \frac{\bar{c}_{pr} \mu_r}{\lambda_r}. \tag{33}$$

(3) The Liao correlation [63] developed for predicting the heat transfer of heating supercritical carbon dioxide flowing in horizontal mini/micro channels with 0.50, 0.70, 1.10, 1.40, 1.55 and 2.16 mm inner diameters. Its formula is as follows:

$$Nu_{gc,rw} = 0.128 Re_{rw}^{0.8} Pr_{rw}^{0.3} (\frac{Gr_r}{Re_h^2})^{0.205} (\frac{\rho_h}{\rho_{rw}})^{0.437} (\frac{\bar{c}_{ph}}{c_{phw}})^{0.411} \tag{34}$$

where Gr_r denotes the Grashof number of the refrigerant in the gas cooler, defined as

$$Gr_r = \frac{(\rho_{rw} - \rho_r)\rho_r g D_{gc,tube,inner}^3}{\mu_r^2}. \tag{35}$$

(4) The Bruch correlation [64] developed for predicting the HTC of cooling supercritical carbon dioxide flowing in a vertical U-tube with 6 mm inner diameter. Its formulas are as follows:

$$Nu_{gc,r} = Nu_{fc,r}[1 - 75(\frac{Gr_r}{Re_r^{2.7}})^{0.46}] \quad if \ \frac{\overline{Gr}_r}{Re_r^{2.7}} < 4.2 \cdot 10^{-5},$$
$$Nu_{gc,r} = Nu_{fc,r}[13.5(\frac{Gr_r}{Re_r^{2.7}})^{0.40}] \quad if \ \frac{\overline{Gr}_r}{Re_r^{2.7}} > 4.2 \cdot 10^{-5}. \tag{36}$$

Here $\overline{Gr}_r$ denotes the average Grashof number of the refrigerant in the gas cooler, defined as

$$\overline{Gr}_r = \frac{(\rho_r - \overline{\rho}_r)\rho_r g D_{gc,tube,inner}^3}{\mu_r^2} \tag{37}$$

where $\overline{\rho}_r$ denotes the average density of the refrigerant, which can be approximated by the following equation [24],

$$\overline{\rho}_r = (\rho_{rw} + \rho_r)/2 \quad if \ T_{rw} > T_{pc} \ or \ T_r < T_{pc},$$
$$\overline{\rho}_r = \frac{\rho_r(T_r - T_{pc}) + \rho_{rw}(T_{pc} - T_w)}{T_r - T_{rw}} \quad if \ T_{rw} < T_{pc} < T_r. \tag{38}$$

Actually, comparing the combined term of these two non-dimensional numbers, $\frac{Gr_r}{Re_r^{2.7}}$, with a constant value, selected by Bruch as $4.2 \cdot 10^{-5}$, was proposed by Jackson and Hall [65] as a simplified criterion for judging whether the buoyancy force would play a significant role in influencing the HTC or not. $Nu_{fc,r,j}$ denotes the forced convection Nusselt number of the refrigerant at the tube side of the jth segment of the gas cooler which is calculated as

$$Nu_{fc,r} = 0.0183 Re_r^{0.82} \overline{Pr}_r (\frac{\rho_r}{\rho_{rw}})^{-0.3}. \tag{39}$$

(5) The Huai correlation [66] developed for predicting the HTC of cooling supercritical carbon dioxide flowing in multi-port minichannels with 1.31 mm inner diameter. Its formula is as follows:

$$Nu_{gc,rw} = 0.0222 Re_{rw}^{0.8} Pr_{rw}^{0.3} (\frac{\rho_r}{\rho_{rw}})^{-1.47} (\frac{\bar{c}_{ph}}{c_{phw}}). \tag{40}$$

(6) The Peeters friction-heat transfer analogy relation [67] derived for predicting the HTC of various supercritical working fluids in combination with the Petrov friction factor [68]. Its formula is as follows:

$$Nu_{gc,r} = \frac{C_f}{2} Re_r (0.7 \frac{\overline{Pr}_r}{Pr_{rw}^{2/3}} + 0.3 \frac{\overline{Pr}_r}{Pr_h^{2/3}}). \tag{41}$$

Here C_f denotes the skin friction coefficient of the refrigerant flowing inside the gas cooler, which is estimated based on the correlation developed by Petrov and Popov [69],

$$C_f = C_{f,iso}[(\frac{\mu_{rw}}{\mu_r})^{(1/4)} + (\frac{\rho_{rw}}{\rho_r})^{(1/3)}|\frac{C_{f,ac}}{C_{f,iso}}|] \tag{42}$$

where

$$C_{f,ac} = \frac{8\phi_{gc}\beta_h}{G_r c_{ph}}, \tag{43}$$

and

$$C_{f,iso} = 0.079 Re_h^{-1/4} \quad if \ Re_r \leq 10^4,$$
$$C_{f,iso} = [1.58 \ln(Re_h) - 3.28]^{-2} \quad if \ Re_h > 10^4. \tag{44}$$

Fig. A.1 to A.2 show the results of one-dimensional calculation for the heat transfer characteristics of the gas cooler in ammonia supercritical heat pump cycles. Their only difference with Fig. 9 to 11 is in determining the heat transfer coefficient of the working fluid—the Bruch correlation [64] used in Section 3.2 is replaced by the aforementioned six correlations in order. It is found that all cases using different correlations predict the same overall trends for the curves in these plots, which have been depicted in detail in Section 3.2 of the main text. However, the obtained total lengths of the gas cooler range from 20 to 55 m, while the maximum heat transfer coefficient on the ammonia side ranges from approximately 450 W/(m² K) to 8000 W/(m² K). Moreover, the spikes of the ammonia side HTC just behind the pseudo-critical point of ammonia display quite distinct shapes. Specifically, the Huai correlation predicts two spikes, the Swenson, Petukhov, Bruch, and Cui correlations predict flat spikes while the Peeters+Petrov correlations predict very acute spikes. It also worth
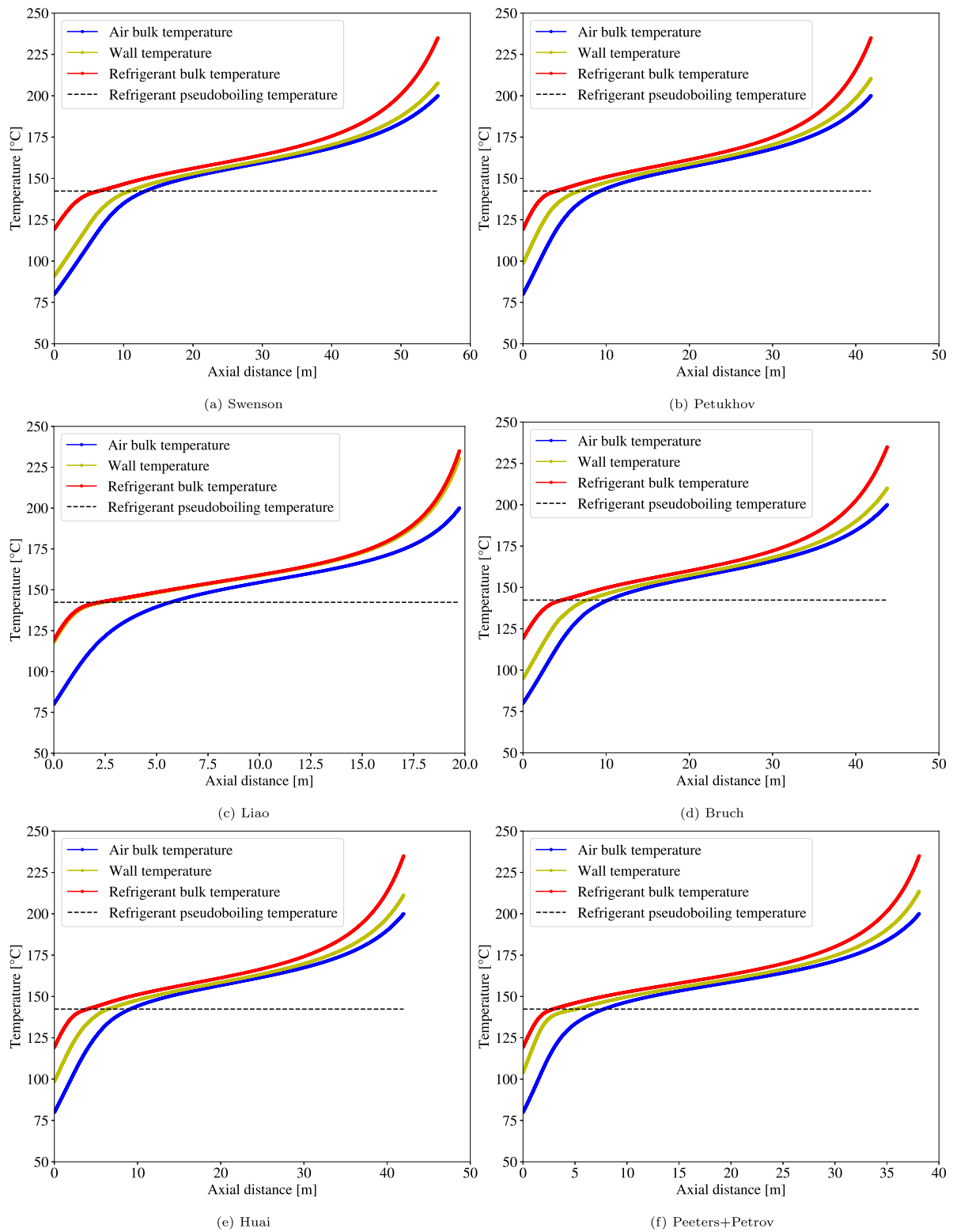
Fig. A.1. Axial temperature distribution in the gas cooler for Ammonia predicted by different supercritical heat transfer correlations.

attention that contrary to Fig. 11(d), all the six correlations predicts lower HTC at the refrigerant side than the air side after the peaks. Unfortunately, without corresponding experimentally measured data as the benchmark, there is no reliable criterion to decide which correlation is most appropriate. Therefore, it is suggested that in the future, more work should be done to provide experimentally measured or DNS simulated data for the supercritical heat transfer performance of R1233zd(E), R1336mzz(Z), n-Butane and ammonia, after then update the existing supercritical heat transfer correlations or developing new ones based on these data.
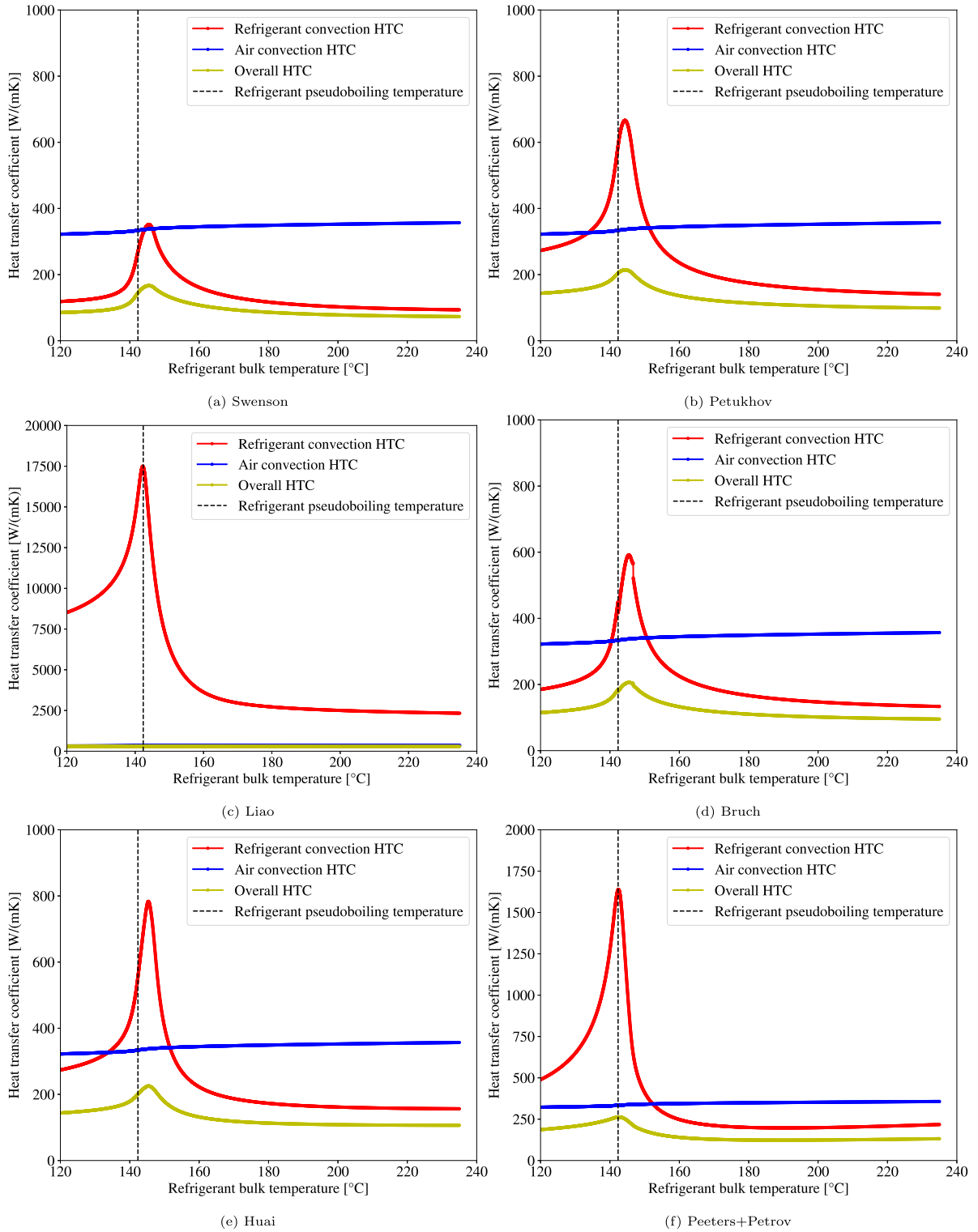
Fig. A.2. Axial HTC distribution in the gas cooler for Ammonia predicted by different supercritical heat transfer correlations.

Appendix C. Zero-dimensional calculation for the evaporator

Since the heat source in the evaporator is assumed to be isothermal at 88 °C, only the working fluid side HTC needs to be calculated for the heat transfer characteristics of the evaporator. The mass flux of the working fluid in the evaporator is assumed to be the same as in the gas cooler. As the refrigerant at the outlet of the evaporator is assumed to be saturated vapor, its quality is one; while the quality of the refrigerant at the inlet of the evaporator is inherited value from the results of thermodynamic performance analysis for the transcritical heat pump cycles. Although there is an abundance of published flow boiling correlations available [70], to avoid bringing in extra assumptions the Schrock correlation [71] is selected owing to its simplicity,

$$Nu_{ev,r} = 170 Re_l^{0.8} Pr_l^{1/3} [Bo_{ev} + 1.50 \times 10^{-4} X_{tt}] \tag{45}$$

where X_{tt} is the Lockhart–Martinelli parameter [72], defined as

$$X_{tt} = (\frac{\mu_l}{\mu_g})^{0.1}(\frac{v_l}{v_g})^{0.5}(\frac{1}{\chi} - 1)^{0.9}. \tag{46}$$

Re_l denotes the liquid phase Reynolds number of refrigerant in the evaporator, defined similarly as in Eq. (5) but with the characteristic length of the evaporator. Pr_l denotes the liquid phase Prandtl number of refrigerant in the evaporator, defined similarly as in Eq. (6) but with the liquid phase properties of the refrigerant. Bo_{ev} denotes the boiling number of the evaporator, which is defined as

$$Bo_{ev,r} = \frac{\phi_{ev}}{h_{lg}\dot{m}_r}. \tag{47}$$

The obtained HTC is then used for determining the length of the evaporator.

For the pressure drop in the evaporator, again only the working fluid side is considered. The classic two-phase fluid pressure drop calculation method based on the Lockhart–Martinelli parameter [72] is adopted, so

$$\Delta P_{ev,r} = \sum_{j=1}^{N}[2\phi_{ev,l}^2 f_{ev,l} \frac{L_{ev}}{D_{ev,tube,inner}(1-\chi)^2} \frac{G_r^2}{\rho_l}], \tag{48}$$

where $\phi_{ev,l}$ denotes the two-phase frictional pressure drop multiplier. It can be evaluated as

$$\phi_{ev,l} = (1.376 + \frac{7.242}{X_{tt}^{1.655}}). \tag{49}$$

$f_{ev,l}$ is the Blausius friction factor [73]. It can be evaluated as

$$f_{ev,l} = 0.0791 Re_l^{-0.25}. \tag{50}$$

References

[1] European Environment Agency. Decarbonising heating and cooling — a climate imperative. 2023.
[2] de Boer R, Marina A, Zühlsdorf B, Arpagaus C, Bantle M, Wik V, et al. Strengthening industrial heat pump innovation: Decarbonizing industrial heat. 2020.
[3] European Commision. A roadmap for moving to a competitive low carbon economy. 2011.
[4] Lazard. Levelized cost of energy – version 16.0. 2023, https://www.lazard.com/media/typdgxmm/lazards-lcoeplus-april-2023.pdf. [Accessed: 23 June 2023].
[5] Department of Energy in United States. Heat pump systems - energy saver. 2023.
[6] Mateu-Royo C, Arpagaus C, Mota-Babiloni A, Navarro-Esbrí J, Bertsch SS. Advanced high temperature heat pump configurations using low GWP refrigerants for industrial waste heat recovery: A comprehensive study. Energy Convers Manag 2021;229:113752.
[7] Naegler T, Simon S, Klein M, Gils HC. Quantification of the European industrial heat demand by branch and temperature level. Int J Energy Res 2015;39(15):2019–30.
[8] Schmitz-Schug I, Kulozik U, Foerst P. Modeling spray drying of dairy products–Impact of drying kinetics, reaction kinetics and spray drying conditions on lysine loss. Chem Eng Sci 2016;141:315–29.
[9] Atkins MJ, Walmsley MR, Neale JR. Integrating heat recovery from milk powder spray dryer exhausts in the dairy industry. Appl Therm Eng 2011;31(13):2101–6.
[10] Chua KJ, Chou SK, Yang W. Advances in heat pump systems: A review. Appl Energy 2010;87(12):3611–24.
[11] Jiang J, Hu B, Wang R, Deng N, Cao F, Wang C-C. A review and perspective on industry high-temperature heat pumps. Renew Sustain Energy Rev 2022;161:112106.
[12] Fukuda S, Kondou C, Takata N, Koyama S. Low GWP refrigerants R1234ze(E) and R1234ze(Z) for high temperature heat pumps. Int J Refrig 2014;40:161–73.
[13] Bamigbetan O, Eikevik TM, Nekså P, Bantle M, Schlemminger C. The development of a hydrocarbon high temperature heat pump for waste heat recovery. Energy 2019;173:1141–53.
[14] Kosmadakis G, Arpagaus C, Neofytou P, Bertsch S. Techno-economic analysis of high-temperature heat pumps with low-global warming potential refrigerants for upgrading waste heat up to 150 °C. Energy Convers Manage 2020;226:113488.
[15] Abedini H, Vieren E, Demeester T, Beyne W, Lecompte S, Quoilin S, et al. A comprehensive analysis of binary mixtures as working fluid in high temperature heat pumps. Energy Convers Manage 2023;277:116652.
[16] Nekså P. CO2 heat pump systems. Int J Refrig 2002;25(4):421–7.
[17] Austin BT, Sumathy K. Transcritical carbon dioxide heat pump systems: A review. Renew Sustain Energy Rev 2011;15(8):4013–29.
[18] Schmidt E, Klöcker K, Flacke N, Steimle F. Applying the transcritical CO2 process to a drying heat pump. Int J Refrig 1998;21(3):202–11.
[19] Banuti D. Crossing the Widom-line–supercritical pseudo-boiling. J Supercrit Fluids 2015;98:12–6.
[20] Maxim F, Karalis K, Boillat P, Banuti DT, Marquez Damian JI, Niceno B, et al. Thermodynamics and dynamics of supercritical water pseudo-boiling. Adv Sci 2021;8(3):2002312.
[21] Peeters J. On the effect of pseudo-condensation on the design and performance of supercritical CO2 gas chillers. Int J Heat Mass Transfer 2022;186:122441.
[22] Jackson J. Models of heat transfer to fluids at supercritical pressure with influences of Buoyancy and acceleration. Appl Therm Eng 2017;124:1481–91.
[23] Forooghi P, Hooman K. Experimental analysis of heat transfer of supercritical fluids in plate heat exchangers. Int J Heat Mass Transfer 2014;74:448–59.
[24] Bae JH, Yoo JY, Choi H. Direct numerical simulation of turbulent supercritical flows with heat transfer. Phys Fluids 2005;17(10):105104.
[25] Yoo JY. The turbulent flows of supercritical fluids with heat transfer. Annu Rev Fluid Mech 2013;45:495–525.
[26] United Nations. The Kigali amendment to the Montreal protocol. 2016.
[27] Zühlsdorf B, Jensen JK, Elmegaard B. Heat pump working fluid selection—economic and thermodynamic comparison of criteria and boundary conditions. Int J Refrig 2019;98:500–13.
[28] Aga V, Conte E, Carroni R, Burcker B, Ramond M. Supercritical CO2-based heat pump cycle for electrical energy storage for utility scale dispatchable renewable energy power plants. In: 5th internjational symposium on supercritical CO2 power cycles. 2016, p. 1–10.
[29] Lemmon EW, Bell IH, Huber M, McLinden M. NIST standard reference database 23: Reference fluid thermodynamic and transport properties-REFPROP, version 10.0. 2018.
[30] Dai X, Shi L, Qian W. Review of the working fluid thermal stability for organic rankine cycles. J Therm Sci 2019;28:597–607.
[31] Kim S, Rached W, Abbas L. Performance and stability of E-1233zd in energy recovery applications. In: International refrigeration and air conditioning conference. 2018, p. 1–8.
[32] Kontomaris K. HFO-1336mzz-Z: High temperature chemical stability and use as a working fluid in Organic Rankine cycles. In: International refrigeration and air conditioning conference. 2014, p. 1–10.
[33] Dai X, Shi L, An Q, Qian W. Screening of hydrocarbons as supercritical ORCs working fluids by thermal stability. Energy Convers Manage 2016;126:632–7.
[34] Bell IH, Wronski J, Quoilin S, Lemort V. Pure and pseudo-pure fluid thermophysical property evaluation and the open-source thermophysical property library CoolProp. Ind Eng Chem Res 2014;53(6):2498–508.
[35] Arpagaus C, Bless F, Schiffmann J, Bertsch SS. Multi-temperature heat pumps: A literature review. Int J Refrig 2016;69:437–65.
[36] Liu F, Groll EA, Ren J. Comprehensive experimental performance analyses of an ejector expansion transcritical CO2 system. Appl Therm Eng 2016;98:1061–9.
[37] Gauvin W, Katta S. Basic concepts of spray dryer design. AIChE J 1976;22(4):713–24.
[38] Fiaschi D, Manfrida G, Russo L, Talluri L. Improvement of waste heat recuperation on an industrial textile dryer: Redesign of heat exchangers network and components. Energy Convers Manage 2017;150:924–40.
[39] Holmgren K. Role of a district-heating network as a user of waste-heat supply from various sources–the case of Göteborg. Appl Energy 2006;83(12):1351–67.
[40] Cengel YA, Boles MA, Kanoğlu M. Thermodynamics: an engineering approach. 9th ed.. McGraw-hill New York; 2018.
[41] Kauf F. Determination of the optimum high pressure for transcritical CO2-refrigeration cycles. Int J Therm Sci 1999;38(4):325–30.
[42] Liao S, Zhao T, Jakobsen A. A correlation of optimal heat rejection pressures in transcritical carbon dioxide cycles. Appl Therm Eng 2000;20(9):831–41.
[43] Redón A, Navarro-Peris E, Pitarch M, Gonzálvez-Macia J, Corberán J. Analysis and optimization of subcritical two-stage vapor injection heat pump systems. Appl Energy 2014;124:231–40.
[44] Lock A, Hooman K, Guan Z. A detailed model of direct dry-cooling for the supercritical carbon dioxide Brayton power cycle. Appl Therm Eng 2019;163:114390.
[45] Tian R, He S, Wei M, Shi L. The staged development of a horizontal pipe flow at supercritical pressure. Int J Heat Mass Transfer 2021;168:120841.
[46] Cheng L, Ribatski G, Thome JR. Analysis of supercritical CO2 cooling in macro-and micro-channels. Int J Refrig 2008;31(8):1301–16.
[47] ASPEN. Exchanger design & rating V12.0. 2020.
[48] Digiovanni MA, WEBB RL. Uncertainty in effectiveness-NTU calculations for crossflow heat exchangers. Heat Transf Eng 1989;10(3):61–70.
[49] Tubular Exchanger Manufactures Association. 10-Th TEMA standard. 2022.
[50] American Society of Mechanical Engineers. ASME B31.1 power piping. 2001.
[51] Browne M, Bansal P. An elemental NTU-ε model for vapour-compression liquid chillers. Int J Refrig 2001;24(7):612–27.
[52] Yoon SH, Kim JH, Hwang YW, Kim MS, Min K, Kim Y. Heat transfer and pressure drop characteristics during the in-tube cooling process of carbon dioxide in the supercritical region. Int J Refrig 2003;26(8):857–64.
[53] Žukauskas A. Heat transfer from tubes in crossflow. In: Advances in heat transfer, vol. 8, Elsevier; 1972, p. 93–160.

[54] Fang X, Bullard CW, Hrnjak PS. Heat transfer and pressure drop of gas coolers. ASHRAE Trans 2001;107(1):255–66.

[55] Holman J. Heat transfer. 10th ed.. McGraw-Hill; 2010.

[56] Bejan A. Entropy generation minimization: the method of thermodynamic optimization of finite-size systems and finite-time processes. CRC Press; 2013.

[57] Alefeld G. Efficiency of compressor heat pumps and refrigerators derived from the second law of thermodynamics. Int J Refrig 1987;10(6):331–41.

[58] Song Y, Cao F. The evaluation of optimal discharge pressure in a water-precooler-based transcritical CO2 heat pump system. Appl Therm Eng 2018;131:8–18.

[59] Goula AM, Adamopoulos KG. Spray drying performance of a laboratory spray dryer for Tomato powder preparation. Drying Technol 2003;21(7):1273–89.

[60] Yamagata K, Nishikawa K, Hasegawa S, Fujii T, Yoshida S. Forced convective heat transfer to supercritical water flowing in tubes. Int J Heat Mass Transfer 1972;15(12):2575–93.

[61] Swenson H. Heat transfer to supercritical water in Smooth-Bore tubes. J Heat Transf 1965;87:477–84.

[62] He J, Dang C, Hihara E. Experimental investigation of heat transfer to supercritical R245fa flowing vertically upward in a circular tube. Int J Heat Mass Transfer 2018;127:286–95.

[63] Liao S, Zhao T. Measurements of heat transfer coefficients from supercritical carbon dioxide flowing in horizontal mini/micro channels. J Heat Transf 2002;124(3):413–20.

[64] Bruch A, Bontemps A, Colasson S. Experimental investigation of heat transfer of supercritical carbon dioxide flowing in a cooled vertical tube. Int J Heat Mass Transfer 2009;52(11–12):2589–98.

[65] Jackson J, WB H. Influences of buoyancy on heat transfer to fluids flowing in vertical tubes under turbulent conditions. In: Turbulent forced convection in channels and bundles, vol. 2, Hemisphere; 1979, p. 613–64.

[66] Huai X, Koyama S, Zhao T. An experimental study of flow and heat transfer of supercritical carbon dioxide in multi-port mini channels under cooling conditions. Chem Eng Sci 2005;60(12):3337–45.

[67] Peeters J, Rohde M. A heat transfer-friction analogy for fluids at supercritical pressure. J Supercrit Fluids 2019;150:75–85.

[68] Ehsan MM, Guan Z, Klimenko A. A comprehensive review on heat transfer and pressure drop characteristics and correlations with supercritical CO2 under heating and cooling applications. Renew Sustain Energy Rev 2018;92:658–75.

[69] Petrov N, Popov V. Heat transfer and hydraulic resistance with turbulent flow in a tube of water at supercritical parameters of state. Therm Eng 1988;35(10):577–80.

[70] Collier JG, Thome JR. Convective boiling and condensation. Clarendon Press; 1994.

[71] Schrock V, Grossman L. Forced convection boiling in tubes. Nucl Sci Eng 1962;12(4):474–81.

[72] Lockhart W. Proposed correlation of data for isothermal two-phase, two-component flow in pipes. Chem Eng Progr 1949;45(1):39–48.

[73] Kundu PK, Cohen IM, Dowling DR. Fluid mechanics. 5th ed.. Academic Press; 2015.